

# Nuclear modulation effects in “2+1” electron spin-echo correlation spectroscopy

Arnold Raitsimring

*Department of Chemistry, University of Arizona, Tucson, Arizona 85721*

Richard H. Crepeau and Jack H. Freed

*Baker Laboratory of Chemistry, Cornell University, Ithaca, New York 14853*

(Received 20 January 1995; accepted 9 March 1995)

This work represents the synthesis of the 2+1 pulse sequence for the study of electron spin-echo envelope modulation (ESEEM) with the technique of spin-echo correlated spectroscopy (SECSY), which has previously been used to study nuclear modulation by two-dimensional Fourier transform ESR methods. This example of “pulse adjustable” spectroscopy, wherein the pulse width and pulse amplitude of the second pulse in a three pulse sequence are introduced as adjustable parameters, leads to enhanced resolution to the key features of the nuclear modulation that are important for structural studies. This is demonstrated in studies on (i) a single crystal of irradiated malonic acid and (ii) a frozen solution of diphenylpicrylhydrazyl in toluene. In particular, it is shown for (i) how the nuclear modulation cross peaks can be preferentially enhanced relative to the autopeaks and to the matrix proton peaks, and also how the autopeaks can be significantly suppressed to enhance resolution for low-frequency cross peaks. For (ii) the low-frequency  $^{14}\text{N}$  nuclear modulation could be suppressed leaving just the high-frequency matrix  $^1\text{H}$  modulation. Additionally, the  $T_2$  homogeneous linewidth broadening in the  $f_1$  frequency direction is removed in 2+1 SECSY. These features significantly improve resolution to the modulation decay, which is the main observable utilized for distance measurements by ESEEM, compared to SECSY. A simple example of a distance measurement to matrix protons is presented for (ii). It is shown that a major advantage of the 2D format is that the full spin-echo shape is collected, which permits one to study how the effect of the nuclear modulation upon the echo varies with evolution time  $t_1$  after the first pulse, and thereby to detect the important modulation features. Additionally it allows for correlating the modulation cross peaks in making spectral assignments. A detailed quantitative theory for 2+1 SECSY is also presented. In general, very good agreement between experiment and theoretical simulations is obtained. © 1995 American Institute of Physics.

## I. INTRODUCTION

Electron-spin-echo envelope modulation (ESEEM) spectroscopy has become a popular method for the investigation of electron–nuclear interactions that are not resolved in continuous wave EPR spectroscopy.<sup>1,2</sup> Until recently ESEEM spectroscopy was mainly based on the use of two and three pulse sequences. In the last decade a number of new pulse sequences as well as new technologies have been developed that substantially improve the resolution and sensitivity in the study of ESEEM. For instance, a four pulse train known as HYSORE<sup>3,4</sup> allows one to correlate the nuclear transition frequencies which belong to the same paramagnetic site; a five pulse sequence<sup>5</sup> allows one to separate the modulated part of the spin-echo signal from the nonmodulated part; and soft ESEEM<sup>6,7</sup> allows one to selectively excite the electron spin transitions. Two-dimensional Fourier transform (2D-FT) ESR spectroscopy<sup>8–12</sup> allows one to substantially improve the frequency resolution of the nuclear modulation as a result of the correlation of the frequencies that is obtained in such experiments as spin-echo correlated spectroscopy (SECSY) and in providing the full shape of the spin-echo signal.

In order to further develop the capabilities of ESEEM spectroscopy we describe in this paper the new technique of 2+1 SECSY-ESR. The principle difference between this technique and those noted above is in the method of forming

the modulation. In 2+1 SECSY-ESR the modulation is developed *during* the action of a pulse, whereas in the other techniques it develops in the time intervals between pulses. As a result, additional experimental parameters appear, viz. the duration and amplitude of the +1 pulse, which allows one to select and optimize the modulation from the particular nuclear frequencies of interest. It is based upon a synthesis of the 2D-FT technique of SECSY-ESR with the basic 2+1 pulse sequence (cf. Fig. 1), which is a three pulse sequence wherein the second pulse is the +1 pulse.<sup>13</sup> In some respects 2+1 SECSY-ESR is related in spirit to a technique due to Bowman, known as coherent Raman beats which is an alternative to ESEEM in the detection of nuclear coherence.<sup>14,15</sup> That is the +1 pulse must neither be “hard” nor “soft” in order to produce a modulation of the spin-echo signal. Since the nuclear modulation in a 2+1 sequence is caused by partial excitation of the ESR spectrum,<sup>16</sup> analytic expressions for describing this phenomenon are not available for the general case which includes arbitrary types of pulses and the full spin-Hamiltonian. Approximate analytical expressions will be derived for the case of so-called weak electron–nuclear interactions, and they will be used in this paper for a qualitative description of the phenomenon. The accurate theoretical description of modulation effects in 2+1 SECSY is pro-

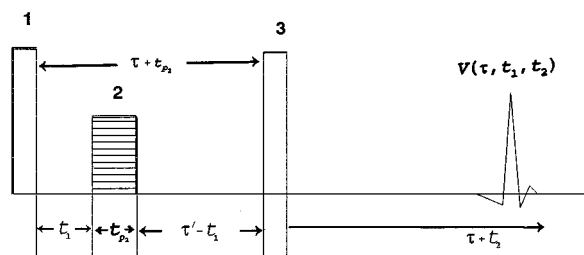


FIG. 1. The 2+1 SECSY pulse sequence. The variable time intervals are  $t_1$  (position of +1 pulse) and  $t_2$  (spin-echo shape time coordinate).

vided in this paper by direct numerical calculation of the spin-echo signal.

In the present work we have studied two systems. The first is an irradiated single crystal of malonic acid, with stable  $\text{CH}(\text{COOH})_2$  radicals. This system has previously been used to characterize the basic ESEEM phenomenon,<sup>17</sup> the study of nuclear modulation by 2D-FT-ESR methods,<sup>8</sup> as well as pulsed electron-nuclear multiple resonance techniques.<sup>18</sup> The second system is a frozen solution of DPPH radicals in toluene which was used to illustrate the ability of the method to preferentially select and enhance nuclear modulations from different nuclear frequencies.

## II. THEORY

As shown in Fig. 1, the first and the third pulses in 2+1 SECSY are separated by the fixed time interval  $\tau + t_{p2}$ , and they generate a primary echo signal. The amplitude of this signal may be varied by changing the interval  $t_1$  between the first pulse and the second or +1 pulse. For each value of  $t_1$  the full spin echo shape is obtained as a function of  $t_2$ . In the following calculations we measure  $t_1$  from the end of the first pulse, and  $t_2$  is measured from the end of the third pulse as  $\tau + t_2$ . The calculations utilize the rotating frame (RF) with a frequency of rotation,  $\omega$  equal to the microwave (mw) frequency with the mw field,  $\mathbf{B}_1$  along the  $x$  axis of the RF. The  $z$  axis of the RF is along the direction of the external magnetic field,  $\mathbf{B}_0$ . We consider a spin system with  $I=1/2$  and  $S=1/2$ . The spin-Hamiltonian of this system is

$$\mathbf{H}_0 = \Delta\omega S_z - \omega_I I_z + AS_z I_z + \frac{1}{2}(BS_z I_+ + B^* S_z I_-), \quad (1)$$

where  $\omega_I$  is the nuclear Zeeman frequency,  $A$  and  $B$  are components of the hyperfine interaction (HFI) tensor, and  $\Delta\omega$  is the difference between the mw and electron spin Zeeman frequencies. The eigenvalues and eigenfunctions of this Hamiltonian can be found elsewhere.<sup>8,19</sup> The energies  $E_i$  and the frequencies  $\Omega_i$  of the four EPR transitions are

$$\begin{aligned} m_s = 1/2 \quad E_1 &= \hbar \frac{\Delta\omega + \omega_\alpha}{2}; & E_2 &= \hbar \frac{\Delta\omega - \omega_\alpha}{2}; \\ m_s = -1/2 \quad E_3 &= \hbar \frac{-\Delta\omega + \omega_\beta}{2}; & E_4 &= \hbar \frac{-\Delta\omega - \omega_\beta}{2}, \\ \Omega_{1,2} &= \Delta\omega \pm \omega_-; & \Omega_{3,4} &= \Delta\omega \pm \omega_+, \end{aligned} \quad (2)$$

$$\omega_\pm = \frac{\omega_\alpha \pm \omega_\beta}{2}; \quad \omega_\alpha = \sqrt{\left(\frac{A}{2} - \omega_I\right)^2 + \frac{|B|^2}{4}};$$

$$\omega_\beta = \sqrt{\left(\frac{A}{2} + \omega_I\right)^2 + \frac{|B|^2}{4}}$$

and their intensities depend on the parameter  $k$ :

$$k = \left[ \frac{\omega_I}{\omega_\alpha \omega_\beta} \right]^2 |B|^2.$$

The eigenvalues and eigenfunctions of this Hamiltonian may be separated into two manifolds, corresponding to  $m_s = 1/2$  and  $m_s = -1/2$ .

Because of its widespread use, we shall use the notation of Mims<sup>20,21</sup> as much as possible. The ESEEM is a modulation of the intensity of the electron-spin echo (ESE) that is produced by the series of microwave pulses. Consequently the ESE amplitude can be calculated from the quantum mechanical expectation value for the raising (or lowering<sup>22</sup>) operators  $\mathbf{S}^+$  (or  $\mathbf{S}^-$ ) for the sample magnetization. This is given in density matrix formalism by

$$V(t) = K \text{Im}\{\text{Tr}[\rho(t)\mathbf{S}^+]\}, \quad (3)$$

where  $V(t)$  is the detected precessing magnetization,  $K$  is largely an instrumental constant, and  $\rho(t)$  is the density matrix evaluated at the time  $t$ . The density matrix  $\rho(t)$  at any time  $t$  can be calculated from its value at an earlier time by the application of a series of unitary operators describing the interactions to which the spin system is subjected. For a 2+1 train, (cf. Fig. 1), the density matrix at the time  $\tau + t_2$  after the third pulse is related to the initial density matrix  $\rho_0$  by

$$\begin{aligned} \rho(\tau + t_2, t_1, \tau) &= \mathbf{R}^+ \rho \mathbf{R} = \mathbf{R}_{\tau+t_2}^+ \mathbf{R}_{N_3}^+ \mathbf{R}_{\tau-t_1}^+ \mathbf{R}_{N_2}^+ \mathbf{R}_{t_1}^+ \mathbf{R}_{N_1}^+ \\ &\times \rho_0 \mathbf{R}_{N_1} \mathbf{R}_{t_1} \mathbf{R}_{N_2} \mathbf{R}_{\tau-t_1} \mathbf{R}_{N_3} \mathbf{R}_{\tau+t_2}, \end{aligned} \quad (4)$$

where  $\mathbf{R}_i$  is the free precession operator,  $\exp(i\mathbf{H}_0 t/\hbar)$ , describing the evolution of the density matrix under the influence of the static spin-Hamiltonian  $\mathbf{H}_0$ . Matrices  $\mathbf{R}_{N_i}$  describe the evolution or nutation during the  $i$ th pulse,  $\mathbf{R}_{N_i} = \exp[i(\mathbf{H}_0 + \mathbf{H}_1)t_{p_i}/\hbar]$ , and  $t_{p_i}$  is the duration of the  $i$ th pulse.  $\mathbf{R}^+$  is Hermitian conjugate of  $\mathbf{R}$ . Note that we can write

$$\mathbf{H}_1 = \hbar \frac{\omega_{N_i}}{2} \begin{bmatrix} \mathbf{0} & \mathbf{M} \\ \mathbf{M}^+ & \mathbf{0} \end{bmatrix},$$

where  $\omega_{N_i}$  is the amplitude of the  $i$ th pulse. For further formal calculations a convenient basis set is one in which  $\mathbf{H}_0$  is block-diagonal and each block corresponds to one electron spin manifold. In this representation  $\mathbf{S}^+$  can be represented as

$$\mathbf{S}^+ = \begin{bmatrix} \mathbf{0} & \mathbf{M} \\ \mathbf{0} & \mathbf{0} \end{bmatrix},$$

where submatrix  $\mathbf{M}$  maps nuclear spin eigenvectors in one electron spin manifold into the nuclear spin eigenvector of the other manifold. In this representation

$$\begin{aligned}
\mathbf{R}_{N_m} &= \begin{bmatrix} \mathbf{T}_m & \mathbf{U}_m \\ \mathbf{V}_m & \mathbf{W}_m \end{bmatrix}; \quad \mathbf{R}_t = \begin{bmatrix} \mathbf{P}_t & \mathbf{0} \\ \mathbf{0} & \mathbf{Q}_t \end{bmatrix}; \quad \rho_0 = \begin{bmatrix} \mathbf{A}_+ & \mathbf{0} \\ \mathbf{0} & \mathbf{A}_- \end{bmatrix}, & \mathbf{T}_m = \mathbf{W}_m = \cos \frac{(\omega_{N_m} t_{p_m})}{2} \mathbf{E}, \\
\mathbf{P}_t &= \Pi_t \exp\left(i \frac{\Delta\omega}{2} t\right); & \mathbf{U}_m = i\mathbf{M} \times \sin \frac{(\omega_{N_m} t_{p_m})}{2}, \quad \mathbf{V}_m = i\mathbf{M}^+ \times \sin \frac{\omega_{N_m} t_{p_m}}{2}, \\
\Pi_t &= \begin{bmatrix} \exp\left(i \frac{\omega_\alpha}{2} t\right) & 0 \\ 0 & \exp\left(-i \frac{\omega_\alpha}{2} t\right) \end{bmatrix}, & (5) \\
\mathbf{Q}_t &= \mathbf{Y}_t \exp\left(-i \frac{\Delta\omega}{2} t\right); \\
\mathbf{Y}_t &= \begin{bmatrix} \exp\left(i \frac{\omega_\beta}{2} t\right) & 0 \\ 0 & \exp\left(-i \frac{\omega_\beta}{2} t\right) \end{bmatrix},
\end{aligned}$$

where  $\omega_\alpha$  and  $\omega_\beta$  are determined by Eq. (2) and represent the frequencies of nuclear transitions. The submatrices  $\mathbf{A}_+$  and  $\mathbf{A}_-$  in the prepulse density matrix  $\rho_0$  in the high-temperature approximation are

$$\mathbf{A}_\pm = (1 \pm q)\mathbf{E}; \quad q = \frac{\hbar\omega}{2kT},$$

where  $\mathbf{E}$  is the unit matrix. For further evaluation, we also represent submatrices of rotational operators  $\mathbf{R}_{Ni}$  for the ‘‘hard’’ pulse limit, i.e., for the case when  $\mathbf{H}_1 \gg \mathbf{H}_0$ :

where  $t_{pm}$  is the duration of the  $m$ th pulse.

Performing the multiplication of the free precession and rotational operators we have for the general case from Eq. (5):

$$\begin{aligned}
\mathbf{R}_{1,1} &= [(\mathbf{T}_1 \mathbf{P}_{t_1} \mathbf{T}_2 + \mathbf{U}_1 \mathbf{Q}_{t_1} \mathbf{V}_2) \mathbf{P}_{\tau-t_1} \mathbf{T}_3 \\
&\quad + (\mathbf{T}_1 \mathbf{P}_{t_1} \mathbf{U}_2 + \mathbf{U}_1 \mathbf{Q}_{t_1} \mathbf{W}_2) \mathbf{Q}_{\tau-t_1} \mathbf{V}_3] \mathbf{P}_{\tau+t_2}, \\
\mathbf{R}_{1,2} &= [(\mathbf{T}_1 \mathbf{P}_{t_1} \mathbf{T}_2 + \mathbf{U}_1 \mathbf{Q}_{t_1} \mathbf{V}_2) \mathbf{P}_{\tau-t_1} \mathbf{U}_3 \\
&\quad + (\mathbf{T}_1 \mathbf{P}_{t_1} \mathbf{U}_2 + \mathbf{U}_1 \mathbf{Q}_{t_1} \mathbf{W}_2) \mathbf{Q}_{\tau-t_1} \mathbf{W}_3] \mathbf{Q}_{\tau+t_2}, \\
\mathbf{R}_{2,1} &= [(\mathbf{V}_1 \mathbf{P}_{t_1} \mathbf{T}_2 + \mathbf{W}_1 \mathbf{Q}_{t_1} \mathbf{V}_2) \mathbf{P}_{\tau-t_1} \mathbf{T}_3 \\
&\quad + (\mathbf{V}_1 \mathbf{P}_{t_1} \mathbf{U}_2 + \mathbf{W}_1 \mathbf{Q}_{t_1} \mathbf{W}_2) \mathbf{Q}_{\tau-t_1} \mathbf{V}_3] \mathbf{P}_{\tau+t_2}, \\
\mathbf{R}_{2,2} &= [(\mathbf{V}_1 \mathbf{P}_{t_1} \mathbf{T}_2 + \mathbf{W}_1 \mathbf{Q}_{t_1} \mathbf{V}_2) \mathbf{P}_{\tau-t_1} \mathbf{U}_3 \\
&\quad + (\mathbf{V}_1 \mathbf{P}_{t_1} \mathbf{U}_2 + \mathbf{W}_1 \mathbf{Q}_{t_1} \mathbf{W}_2) \mathbf{Q}_{\tau-t_1} \mathbf{W}_3] \mathbf{Q}_{\tau+t_2}.
\end{aligned} \tag{7a}$$

To check this expression let us turn off the second pulse, i.e., put  $\omega_{N2} = 0$  and  $t_{p2} = 0$ . In this case  $\mathbf{V}_2 = \mathbf{U}_2 = \mathbf{0}$ ;  $\mathbf{T}_2 = \mathbf{W}_2 = \mathbf{E}$ . Taking into account that  $\mathbf{P}_{t1} \mathbf{P}_{\tau-t1} = \mathbf{P}_\tau$  and  $\mathbf{Q}_{t1} \mathbf{Q}_{\tau-t1} = \mathbf{Q}_\tau$  we obtain exactly the same rotational operator as Eq. (24) in Mims<sup>20</sup>:

$$\mathbf{R} = \begin{bmatrix} \mathbf{T}_1 \mathbf{P}_\tau \mathbf{T}_3 \mathbf{P}_{\tau+t_2} + \mathbf{U}_1 \mathbf{Q}_\tau \mathbf{V}_3 \mathbf{P}_{\tau+t_2} & \mathbf{T}_1 \mathbf{P}_\tau \mathbf{U}_3 \mathbf{Q}_{\tau+t_2} + \mathbf{U}_1 \mathbf{Q}_\tau \mathbf{W}_3 \mathbf{Q}_{\tau+t_2} \\ \mathbf{V}_1 \mathbf{P}_\tau \mathbf{T}_3 \mathbf{P}_{\tau+t_2} + \mathbf{W}_1 \mathbf{Q}_\tau \mathbf{V}_3 \mathbf{P}_{\tau+t_2} & \mathbf{V}_1 \mathbf{P}_\tau \mathbf{U}_3 \mathbf{Q}_{\tau+t_2} + \mathbf{W}_1 \mathbf{Q}_\tau \mathbf{W}_3 \mathbf{Q}_{\tau+t_2} \end{bmatrix}. \tag{7b}$$

Evaluating Eq. (4) and using the result in Eq. (3) we find that

$$\begin{aligned}
V(t_2, \tau, t_1) &= K \operatorname{Im}\{\operatorname{Tr}[\mathbf{Q}_{\tau+t_2}^+ (\mathbf{U}_3^+ \mathbf{P}_{\tau-t_1}^+ (\mathbf{T}_2^+ \mathbf{P}_{t_1}^+ \mathbf{V}_1^+ + \mathbf{V}_2^+ \mathbf{Q}_{t_1}^+ \mathbf{W}_1^+) + \mathbf{W}_3^+ \mathbf{Q}_{\tau-t_1}^+ (\mathbf{U}_2^+ \mathbf{P}_{t_1}^+ \mathbf{V}_1^+ + \mathbf{W}_2^+ \mathbf{Q}_{t_1}^+ \mathbf{W}_1^+)) \mathbf{A}_- \\
&\quad \times ((\mathbf{V}_1 \mathbf{P}_{t_1} \mathbf{T}_2 + \mathbf{W}_1 \mathbf{Q}_{t_1} \mathbf{V}_2) \mathbf{P}_{\tau-t_1} \mathbf{T}_3 + (\mathbf{V}_1 \mathbf{P}_{t_1} \mathbf{U}_2 + \mathbf{W}_1 \mathbf{Q}_{t_1} \mathbf{W}_2) \mathbf{Q}_{\tau-t_1} \mathbf{V}_3) \mathbf{P}_{\tau+t_2} \mathbf{M} \\
&\quad + \mathbf{Q}_{\tau+t_2}^+ (\mathbf{U}_3^+ \mathbf{P}_{\tau-t_1}^+ (\mathbf{T}_2^+ \mathbf{P}_{t_1}^+ \mathbf{T}_1^+ + \mathbf{V}_2^+ \mathbf{Q}_{t_1}^+ \mathbf{U}_1^+) + \mathbf{W}_3^+ \mathbf{Q}_{\tau-t_1}^+ (\mathbf{U}_2^+ \mathbf{P}_{t_1}^+ \mathbf{T}_1^+ + \mathbf{W}_2^+ \mathbf{Q}_{t_1}^+ \mathbf{U}_1^+)) \mathbf{A}_+ \\
&\quad \times ((\mathbf{T}_1 \mathbf{P}_{t_1} \mathbf{T}_2 + \mathbf{U}_1 \mathbf{Q}_{t_1} \mathbf{V}_2) \mathbf{P}_{\tau-t_1} \mathbf{T}_3 + (\mathbf{T}_1 \mathbf{P}_{t_1} \mathbf{U}_2 + \mathbf{U}_1 \mathbf{Q}_{t_1} \mathbf{W}_2) \mathbf{Q}_{\tau-t_1} \mathbf{V}_3) \mathbf{P}_{\tau+t_2} \mathbf{M}]\}. \tag{8}
\end{aligned}$$

Mims has pointed out that not all terms of Eq. (8) contribute to the desired spin-echo signals. For this particular case, only those terms in which there is exact cancellation of the electron-spin Zeeman term in the exponentials for  $t_2 \approx 0$ , while  $\tau$  and  $t_1$  are arbitrary, will contribute to the observed 2+1 signal. (Actually, in the present case one must carefully study the terms giving exact cancellation for  $0 \leq t_2 \leq t_{p2}$ . Our analysis of this shows that for  $\omega_{N2} \ll |\Delta\omega|$  one should use  $t_2 \approx t_{p2}$  but for  $\omega_{N2} \gg |\Delta\omega|$  one should use  $t_2 \approx 0$ . The latter case applies to our experimental studies.) After removing the terms which have no cancellation for  $t_2 \approx 0$  and any  $\tau$ , Eq. (8) becomes

$$\begin{aligned}
V(t_2, \tau, t_1) &= K \operatorname{Im}\{\exp(i\Delta\omega t_2) \\
&\quad \times \operatorname{Tr}[(\mathbf{Y}_{\tau+t_2}^+ \mathbf{U}_3^+ \mathbf{\Pi}_\tau^+ \mathbf{P}_{-t_1}^+ (\mathbf{T}_2^+ \mathbf{P}_{t_1}^+ \mathbf{V}_1^+ + \mathbf{V}_2^+ \mathbf{Q}_{t_1}^+ \mathbf{W}_1^+) \mathbf{A}_- (\mathbf{V}_1 \mathbf{P}_{t_1} \mathbf{U}_2 + \mathbf{W}_1 \mathbf{Q}_{t_1} \mathbf{W}_2) \mathbf{Y}_\tau \mathbf{Q}_{-t_1} \mathbf{V}_3 \mathbf{\Pi}_{\tau+t_2}) \mathbf{M} \\
&\quad + (\mathbf{Y}_{\tau+t_2}^+ \mathbf{U}_3^+ \mathbf{\Pi}_\tau^+ \mathbf{P}_{-t_1}^+ (\mathbf{T}_2^+ \mathbf{P}_{t_1}^+ \mathbf{T}_1^+ + \mathbf{V}_2^+ \mathbf{Q}_{t_1}^+ \mathbf{U}_1^+) \mathbf{A}_+ (\mathbf{T}_1 \mathbf{P}_{t_1} \mathbf{U}_2 + \mathbf{U}_1 \mathbf{Q}_{t_1} \mathbf{W}_2) \mathbf{Y}_\tau \mathbf{Q}_{-t_1} \mathbf{V}_3 \mathbf{\Pi}_{\tau+t_2}) \mathbf{M}]\}, \tag{9}
\end{aligned}$$

where uncertainty of the  $t_2$  origin, as we already mentioned, is  $\leq t_{p2}$ . We now select terms independent of  $\Delta\omega t_1$  leading to the final result

$$V(t_2, \tau, t_1) = K \operatorname{Im}\{\exp(i\Delta\omega t_2) \operatorname{Tr}[(\mathbf{Y}_{\tau+t_2}^+ \mathbf{U}_3^+ \mathbf{\Pi}_{\tau-t_1}^+ \mathbf{T}_2^+ \mathbf{\Pi}_{t_1}^+ \mathbf{V}_1^+ \mathbf{A}_- \mathbf{W}_1 \mathbf{Y}_{t_1} \mathbf{W}_2 \mathbf{Y}_{\tau-t_1} \mathbf{V}_3 \mathbf{\Pi}_{\tau+t_2}) \mathbf{M} + (\mathbf{Y}_{\tau+t_2}^+ \mathbf{U}_3^+ \mathbf{\Pi}_{\tau-t_1}^+ \mathbf{T}_2^+ \mathbf{\Pi}_{t_1}^+ \mathbf{T}_1^+ \mathbf{A}_+ \mathbf{U}_1 \mathbf{Y}_{t_1} \mathbf{W}_2 \mathbf{Y}_{\tau-t_1} \mathbf{V}_3 \mathbf{\Pi}_{\tau+t_2}) \mathbf{M}]\}. \quad (10)$$

Before further evaluation, let us obtain from Eq. (10) some known results. Equation (10) immediately gives the ESEEM for a primary echo (as well as the associated SECSY) if the second pulse is turned off and the first and third pulses are set to be hard pulses, i.e., for submatrices  $\mathbf{T}$ ,  $\mathbf{W}$ ,  $\mathbf{U}$ , and  $\mathbf{V}$  we can use Eq. (6):

$$\begin{aligned} \mathbf{W}_2 = \mathbf{T}_2 = \mathbf{E}, \\ V(\tau, t_2) = \text{SECSY} = K \operatorname{Im}\{\exp(i\Delta\omega t_2) \\ \times \operatorname{Tr}[\mathbf{Y}_{\tau+t_2}^+ \mathbf{U}_3^+ \mathbf{\Pi}_{\tau}^+ \mathbf{V}_1^+ \mathbf{A}_- \mathbf{W}_1 \mathbf{Y}_{\tau} \mathbf{V}_3 \mathbf{\Pi}_{\tau+t_2} \mathbf{M} + \mathbf{Y}_{\tau+t_2}^+ \mathbf{U}_3^+ \mathbf{\Pi}_{\tau}^+ \mathbf{T}_1^+ \mathbf{A}_+ \mathbf{U}_1 \mathbf{Y}_{\tau} \mathbf{V}_3 \mathbf{\Pi}_{\tau+t_2} \mathbf{M}]\} \\ = \frac{K}{2} (2q) \sin(\omega_{N_1} t_{p_1}) \sin^2 \frac{\omega_{N_3} t_{p_3}}{2} \operatorname{Im}\{i \exp(i\Delta\omega t_2) \operatorname{Tr}(\mathbf{Y}_{\tau+t_2}^+ \mathbf{M}^+ \mathbf{\Pi}_{\tau}^+ \mathbf{M} \mathbf{Y}_{\tau} \mathbf{M}^+ \mathbf{\Pi}_{\tau+t_2} \mathbf{M})\}. \end{aligned} \quad (11)$$

Equation (11) with  $t_2=0$  yields the ESEEM in the hard-pulses limit which can be directly compared with the well known result [see, e.g., Eq. (7) in Ref. 23]. For the case  $\Delta\omega=0$ , it exactly corresponds to the expression for the SECSY signal, obtained in Ref. 8 if the phases of the pulses are equal to zero.

Now we consider the case of three hard pulses. Thus we can use the submatrices  $\mathbf{T}_2$  and  $\mathbf{W}_2 = \mathbf{E} \cos(\omega_{N_2} t_{p_2}/2)$  in the hard pulse limit [cf. Eq. (6)]. We immediately see from Eq. (10) that the  $t_1$  dependence disappears and the resulting expression describes the ESEEM of a primary echo, generated by the first and third pulses with an amplitude subjected to the action of the second pulse. It is easy to show that this term is equivalent to the  $A_9\alpha_9$  term in accordance with the classification of Gamliel and Freed<sup>10</sup> [see, e.g., the Appendix, Eqs. (51) and (52)]. In the present notation we have

$$\begin{aligned} V(t_2, \tau) = \frac{K}{2} (2q) \sin(\omega_{N_1} t_{p_1}) \cos^2 \frac{\omega_{N_2} t_{p_2}}{2} \sin^2 \frac{\omega_{N_3} t_{p_3}}{2} \\ \times \operatorname{Im}[-i \exp(i\Delta\omega t_2) \\ \times \operatorname{Tr}(\mathbf{Y}_{\tau+t_2}^+ \mathbf{M}^+ \mathbf{\Pi}_{\tau}^+ \mathbf{M} \mathbf{Y}_{\tau} \mathbf{M}^+ \mathbf{\Pi}_{\tau+t_2} \mathbf{M})]. \end{aligned} \quad (12)$$

Equation (12) shows that in the hard pulse limit the modulation in a 2+1 sequence is absent. To obtain it, the matrices  $\mathbf{T}_2$  and  $\mathbf{W}_2$  must contain off-diagonal elements, which occurs when the second pulse is neither hard nor soft.

For arbitrary pulses let us start with the degenerate case of the absence of HFI to reproduce the classic result of Bloom<sup>24</sup> for the shape of a spin-echo signal in the case of partial excitation. For this case all  $2 \times 2$  submatrices in Eq. (5) degenerate to scalars and  $\omega_\beta = \omega_\alpha = 0$ . The explicit forms of  $\mathbf{U}$ ,  $\mathbf{T}$ ,  $\mathbf{W}$ , and  $\mathbf{V}$  are

$$\mathbf{Y} \rightarrow \mathbf{1}; \mathbf{\Pi} \rightarrow \mathbf{1}; \mathbf{M} \rightarrow \mathbf{1}; \mathbf{U} = \mathbf{V} \rightarrow \beta^*; \mathbf{W} \rightarrow \alpha^*; \mathbf{T} \rightarrow \alpha,$$

$$\alpha_i = \cos \frac{\omega_{\text{eff}_i} t_{p_i}}{2} - i \cos \phi_i \sin \frac{\omega_{\text{eff}_i} t_{p_i}}{2},$$

$$\beta = -i \sin \phi_i \sin \frac{\omega_{\text{eff}_i} t_{p_i}}{2},$$

$$\phi_i = \arctan\left(\frac{\omega_{N_i}}{\Delta\omega}\right); \quad \omega_{\text{eff}} = \sqrt{\omega_{N_i}^2 + \Delta\omega^2}.$$

Then Eq. (10) becomes

$$\begin{aligned} V(t_2) \propto \operatorname{Im}\{\exp(i\Delta\omega t_2) (\mathbf{U}_3^+ \mathbf{T}_2^+ (\mathbf{T}_1^+ \mathbf{U}_1 - \mathbf{V}_1^+ \mathbf{W}_1) \mathbf{W}_2 \mathbf{V}_3)\} \\ = -\operatorname{Im}\{2\alpha_1^* \beta_1^* \alpha_2^{*2} \beta_3^2 \exp(i\Delta\omega t_2)\} \end{aligned} \quad (13)$$

and this result reproduces Eq. (19) of Bloom.<sup>24</sup>

The general case of all three soft pulses is complicated and the rotational operators for arbitrary HFI have no analytical expressions. We shall first consider a simple case wherein the first and third pulses are hard pulses and there is an extremely weak hyperfine interaction,  $B, A \ll \omega_I, \omega_{N_i}$  so that the parameter  $k \ll 1$  [see Eq. (2) and below]. Then using the explicit form of the rotational operator for the second pulse, which was derived in Refs. 16 and 25, we still can get a closed expression. We have to remind the reader that the echo modulation amplitude is proportional to  $k$ , and in the following calculations of echo modulation we shall keep only terms of zero order (primary echo signal amplitude) and first order in  $k$ . With two hard pulses, i.e., the first and third ones, Eq. (10) becomes

$$\begin{aligned} V(\tau, t_2, t_1) = K \frac{2q}{2} \sin(\omega_{N_1} t_{p_1}) \sin^2 \frac{\omega_{N_3} t_{p_3}}{2} \\ \times \operatorname{Im}\{i \exp(i\Delta\omega t_2) \operatorname{Tr}(\mathbf{Y}_{\tau+t_2}^+ \mathbf{M}^+ \mathbf{\Pi}_{\tau-t_1}^+ \\ \times \mathbf{T}_2^+ \mathbf{\Pi}_{t_1}^+ \mathbf{M} \mathbf{Y}_{t_1} \mathbf{W}_2 \mathbf{Y}_{\tau-t_1} \mathbf{M}^+ \mathbf{\Pi}_{\tau+t_2} \mathbf{M})\}. \end{aligned} \quad (14)$$

The explicit forms of  $\mathbf{T}_2$ ,  $\mathbf{W}_2$ , and  $\mathbf{M}$  are<sup>16,25</sup>

$$\begin{aligned}
\mathbf{T}_2 &= \begin{vmatrix} P_1 & i\eta \\ i\eta & P_2^* \end{vmatrix}, \quad \mathbf{W}_2 = \begin{vmatrix} P_2 & -i\eta \\ -i\eta & P_1^* \end{vmatrix}, \quad \mathbf{M} \approx \begin{vmatrix} 1 & \frac{\sqrt{k}}{2} \\ -\frac{\sqrt{k}}{2} & 1 \end{vmatrix}, \\
\mathbf{P}_1 &= \frac{\exp[i(\omega_{\text{eff}} - \omega_I)t_{p_2}/2] + \exp[-i(\omega_{\text{eff}} + \omega_I)t_{p_2}/2]}{2} + \cos \phi \frac{\exp[i(\omega_{\text{eff}} - \omega_I)t_{p_2}/2] - \exp[-i(\omega_{\text{eff}} + \omega_I)t_{p_2}/2]}{2}, \\
\mathbf{P}_2 &= \frac{\exp[i(\omega_{\text{eff}} - \omega_I)t_{p_2}/2] + \exp[-i(\omega_{\text{eff}} + \omega_I)t_{p_2}/2]}{2} - \cos \phi \frac{\exp[i(\omega_{\text{eff}} - \omega_I)t_{p_2}/2] - \exp[-i(\omega_{\text{eff}} + \omega_I)t_{p_2}/2]}{2}, \\
\eta &= -\frac{\sqrt{k}}{4} \omega_{N_2} \sin \phi \left[ \frac{\sin[(\omega_I + \omega_{\text{eff}})t_{p_2}/2]}{\omega_I + \omega_{\text{eff}}} + \frac{\sin[(\omega_I - \omega_{\text{eff}})t_{p_2}/2]}{\sqrt{(\omega_I - \omega_{\text{eff}})^2 + (\omega_{N_2}k)^2/4}} \right].
\end{aligned} \tag{15}$$

The matrices  $\mathbf{T}_2$  and  $\mathbf{W}_2$  may now be represented as a sum of two matrices with diagonal and off-diagonal elements, respectively,

$$\begin{aligned}
\mathbf{T}_2^+ &= \mathbf{X} - i\eta \mathcal{L}, \quad \mathbf{W}_2 = \mathbf{Z} - i\eta \mathcal{L}, \\
\mathcal{L} &= \begin{vmatrix} 0 & 1 \\ 1 & 0 \end{vmatrix}, \quad \mathbf{X} = \begin{vmatrix} P_1^* & 0 \\ 0 & P_2 \end{vmatrix}, \quad \mathbf{Z} = \begin{vmatrix} P_2 & 0 \\ 0 & P_1^* \end{vmatrix}.
\end{aligned} \tag{16}$$

Then Eq. (14) may be written as a sum of three terms:

$$\begin{aligned}
V(\tau, t_2, t_1) &= K \frac{(2q)}{2} \sin(\omega_{N_1} t_{p_1}) \sin^2 \frac{\omega_{N_3} t_{p_3}}{2} \times \{ \text{Im} \{ i \exp(i\Delta\omega t_2) \text{Tr}(\mathbf{Y}_{\tau+t_2}^+ \mathbf{M}^+ \mathbf{\Pi}_{\tau}^+ \mathbf{X} \mathbf{M} \mathbf{Z} \mathbf{Y}_{\tau} \mathbf{M}^+ \mathbf{\Pi}_{\tau+t_2} \mathbf{M}) \} \\
&\quad + \text{Im} \{ \eta \exp(i\Delta\omega t_2) \text{Tr}[\mathbf{Y}_{\tau+t_2}^+ \mathbf{M}^+ [\mathbf{\Pi}_{\tau}^+ \mathbf{X} \mathbf{M} \mathbf{Y}_{t_1} \mathcal{L} \mathbf{Y}_{\tau-t_1} + \mathbf{\Pi}_{\tau-t_1}^+ \mathcal{L} \mathbf{\Pi}_{t_1} \mathbf{M} \mathbf{Y}_{\tau} \mathbf{Z}] \mathbf{M}^+ \mathbf{\Pi}_{\tau+t_2} \mathbf{M}] \} \\
&\quad + \text{Im} \{ -i\eta^2 \exp(i\Delta\omega t_2) \text{Tr}(\mathbf{Y}_{\tau+t_2}^+ \mathbf{M}^+ \mathbf{\Pi}_{\tau-t_1}^+ \mathcal{L} \mathbf{\Pi}_{t_1}^+ \mathbf{M} \mathbf{Y}_{t_1} \mathcal{L} \mathbf{Y}_{\tau-t_1} \mathbf{M}^+ \mathbf{\Pi}_{\tau+t_2} \mathbf{M}) \} \}.
\end{aligned} \tag{17}$$

Actually, Eq. (17) already is an analytical solution of the problem. However, it is useful to simplify further in order to analyze the key features of the modulation in this pulse sequence. Thus we will set  $t_2=0$ . The first term in Eq. (17) has no  $t_1$  dependence and represents the primary echo signal generated by the first and third pulses. The second pulse can only modify its amplitude, but it does not impart any information related to  $t_1$ -dependent nuclear modulation. Direct calculation of the amplitude of the first term gives an expression that is proportional to  $(\alpha_2^*)^2$  in accord with Eq. (13). The second term is responsible for the nuclear modulation at fundamental frequencies,  $\omega_\alpha$  and  $\omega_\beta$ , and the third one contains the combination frequencies. Since the calculations are performed at  $k \ll 1$ , one need only keep in the second term those terms of the sum which are proportional to  $\sqrt{k}$ , given that  $\eta$  is already proportional to  $\sqrt{k}$ . This means that in the Trace evaluation [cf. Eq. (17)] we keep terms in which only one element in the product of the  $M_{ik}$  is allowed to be off-diagonal ( $\sim \sqrt{k}$ ), so the three others must be diagonal ( $M_{ii}=1$ ) [cf. Eq. (15)]. By the same reasoning, for the third term, all elements in the product of the  $M_{ik}$  must be diagonal. Under this condition Eq. (17) is transformed to

$$\begin{aligned}
V(\tau, t_2=0, t_1) &= K \frac{2q}{2} \sin(\omega_{N_1} t_{p_1}) \sin^2 \frac{\omega_{N_3} t_{p_3}}{2} \left\{ \text{Re}[(\alpha_2^*)^2] \right. \\
&\quad + \text{Im} \left\{ \left( \eta \frac{\sqrt{k}}{2} \right) [(P_1^* - P_2)(\cos \omega_\beta t_1 + \cos \omega_\alpha t_1 + \cos[\omega_\beta(\tau - t_1)] + \cos[\omega_\alpha(\tau - t_1)]) \right. \\
&\quad + \cos(\omega_\alpha \tau - \omega_\beta t_1) + \cos(\omega_\beta \tau - \omega_\alpha t_1) - i(P_1^* + P_2)(\sin \omega_\beta t_1 + \sin \omega_\alpha t_1 + \sin \omega_\beta(\tau - t_1) \\
&\quad \left. \left. + \sin \omega_\alpha(\tau - t_1) + \sin(\omega_\alpha \tau - \omega_\beta t_1) + \sin(\omega_\beta \tau - \omega_\alpha t_1)) \right] \right\} - 2\eta^2 \cos(\omega_\alpha - \omega_\beta)t_1 \left. \right\}
\end{aligned} \tag{18}$$

and the final expression is

$$\begin{aligned}
V(\tau, t_2=0, t_1) = & K \frac{2q}{2} \sin(\omega_{N_1} t_{p_1}) \sin^2 \frac{\omega_{N_3} t_{p_3}}{2} \left\{ \text{Re}[(\alpha_2^*)^2] + \left\{ \left( \eta \sqrt{k} \cos \frac{\omega_{\text{eff}} t_{p_2}}{2} \right) (\sin(\omega_{\beta} t_1 - \varpi) + \sin(\omega_{\alpha} t_1 - \varpi)) \right. \right. \\
& + \sin[\omega_{\beta}(\tau - t_1) - \tilde{\omega}] + \sin[\omega_{\alpha}(\tau - t_1) - \tilde{\omega}] + \sin(\omega_{\alpha} \tau - \omega_{\beta} t_1 - \tilde{\omega}) + \sin(\omega_{\beta} \tau - \omega_{\alpha} t_1 - \tilde{\omega}) \left. \left. \right\} \right. \\
& \left. - 2\eta^2 \cos(\omega_{\alpha} - \omega_{\beta}) t_1 \right\}; \quad \tilde{\omega} = \frac{\omega_I t_{p_2}}{2}. \tag{19}
\end{aligned}$$

Equation (19) shows an important feature of the 2+1 sequence: viz. neither the amplitude of the spin-echo nor the amplitude of the nuclear modulation are simply factorable. That means, for example, that the maximum sensitivity to the nuclear modulation will not, in general, be at the maximum of the echo height. Even more important, this structure of Eq. (19) allows one to independently vary the relative importance of the primary echo term vs the modulation terms, such that the former may be set to zero (or at least a small value) with the latter remaining strong. For example, because the amplitude of the primary spin-echo signal (which in Fourier transform yields the autopeaks) is proportional to  $\text{Re}(\alpha_2^*)^2 \approx \cos^2 \omega_{\text{eff}} t_{p_2}/2$ , and a portion of the nuclear modulation amplitude (which results in the nuclear modulation cross peaks), is proportional to  $\sin(\omega_{\text{eff}} t_{p_2})$ , the autopeaks may be substantially suppressed at certain values of  $\omega_{N_2} t_{p_2}$ , i.e., the nominal angle by which the electron spin is rotated leaving mainly just the modulation cross peaks. For the simple case of  $\Delta\omega=0$ , the parameter  $\eta$  [cf. Eq. (15)] responsible for the nuclear modulation depth becomes

$$\begin{aligned}
\eta = & -\frac{\sqrt{k}}{4} \omega_{N_2} \left\{ \frac{\sin[(\omega_I + \omega_{N_2}) t_{p_2}/2]}{\omega_I + \omega_{N_2}} \right. \\
& \left. + \frac{\sin[(\omega_I - \omega_{N_2}) t_{p_2}/2]}{\sqrt{(\omega_I - \omega_{N_2})^2 + (\omega_{N_2} k)^2/4}} \right\}.
\end{aligned}$$

The optimal nuclear modulation amplitude may be reached at  $(\omega_I + \omega_{N_2}) t_{p_2}/2 \approx (2n+1)\pi/2$ , e.g., let  $\omega_{N_2} = \omega_I$  and  $\omega_I t_{p_2} = \pi/2$ . This simple example offers some indication even for the more complicated case of arbitrary HFI, as to how to adjust the parameters of the +1 pulse to obtain the optimal selection or enhancement of the desired nuclear frequencies in an experiment. Actual calculations for a range of parameters and for strong HFI show that the modulation cross peaks are maximized for  $\omega_{N_2} t_{p_2} \approx 2\pi$ . We find a useful general prescription to maximize a given cross peak is to set  $t_{p_2} \approx \omega_I^{-1}$  and vary  $\omega_{N_2}$  such that  $\omega_{N_2} t_{p_2}$  ranges from  $\pi/2$  to  $2\pi$  seeking the optimum rotational angle.

For the more general case, which includes the  $t_2$  dependence [cf. Eq. (14)], one can see that the phase of the nuclear modulation depends on  $t_2$ . For these reasons the best way of performing the 2+1 sequence is by means of a two-dimensional acquisition in  $t_1$  and  $t_2$  which allows one to collect the full modulation pattern of the spin-echo signal. These features will be illustrated below. The general case of arbitrary pulses and arbitrary values of the HFI, as we have

already noted, has no analytical solution. Therefore, numerical calculations of the 2+1—SECSY signal were performed. The numerical calculations may be based on the general Eqs. (3) and (4) or alternatively Eq. (10), wherein the desired echo signal is already selected. In our calculation we started directly from Eqs. (3) and (4), which would more readily permit adapting the computer program for calculating any signal generated by the three pulses. The calculations were performed in a manner similar to the method described in Ref. 26. That is, the free precession periods are determined by  $\mathbf{H}_0$  [Eq. (1)], which was first represented in the spin basis set in which  $\Delta\omega S_z - \omega_I I_z + AS_z I_z$  (of  $\mathbf{H}_0$ ) is diagonal, i.e., the “Zeeman representation.” This representation of  $\mathbf{H}_0$  was then diagonalized, yielding its eigenvalues and the unitary transformation that diagonalizes it,  $\mathbf{O}_0$ . Then the total Hamiltonian  $\mathbf{H}_0 + \mathbf{H}_1$  needed during the pulses was diagonalized yielding its eigenvalues and the associated unitary transformation from the Zeeman representation,  $\mathbf{O}_1$ . Given these transformations we could then obtain the  $\mathbf{R}_{Ni}$  of Eq. (4) in the representation that diagonalized  $\mathbf{H}_0$ , i.e., as  $\mathbf{O}_0^{-1} \mathbf{O}_1 \exp[i\lambda t_{p_i}/\hbar] \mathbf{O}_1^{-1} \mathbf{O}_0$ , where  $\lambda$  is the diagonalized form of  $\mathbf{H}_0 + \mathbf{H}_1$ . The eigenfunctions and eigenvalues of the respective Hamiltonians were obtained by using standard methods (TRED2 and TQLI, cf. Ref. 27). We now write Eqs. (3) and (4) as

$$\begin{aligned}
V_i(t_2, t_1, \tau) = & \sum_{k\dots u} (S_i)_{kl} \exp[-i\epsilon_l(\tau + t_2)] (R_{N_3}^+)_{ln} \\
& \times \exp[-i\epsilon_n(\tau - t_1)] (R_{N_2}^+)_{nm} \exp(-i\epsilon_m t_1) \\
& \times (R_{N_1}^+)_{mj} (S_z)_j (R_{N_1})_{jr} \exp(i\epsilon_r t_1) \\
& \times (R_{N_2})_{ru} \exp[i\epsilon_u(\tau - t_1)] \\
& \times (R_{N_3})_{uk} \exp[i\epsilon_k(\tau + t_2)] \tag{20}
\end{aligned}$$

with  $\epsilon_i = \mathbf{E}_i/\hbar$  and  $\mathbf{S}_i = \mathbf{S}_x, \mathbf{S}_y$ . In Eq. (20) we have utilized the eigenvectors of  $\mathbf{H}_0$  as the basis states with eigenvalues  $E_i$ . (The transformed forms of  $\mathbf{R}_1, \mathbf{R}_2, \mathbf{R}_3$  are implicitly dealt with as we noted above.)

We must now apply the conditions for selection of the desired spin-echo signal that were previously used to go from Eq. (8) [which is a rewritten form of Eqs. (3) and (4)] to Eq. (10). These conditions may now be rewritten as

$$\begin{aligned}
\left. \begin{aligned} |\epsilon_l + \epsilon_n - \epsilon_u - \epsilon_k| \\ |\epsilon_n - \epsilon_m + \epsilon_r - \epsilon_u| \end{aligned} \right\} = 0; \quad \omega_{\alpha}; \quad \omega_{\beta}; \quad \omega_{\alpha} + \omega_{\beta}; \quad |\omega_{\alpha} - \omega_{\beta}|.
\end{aligned}$$

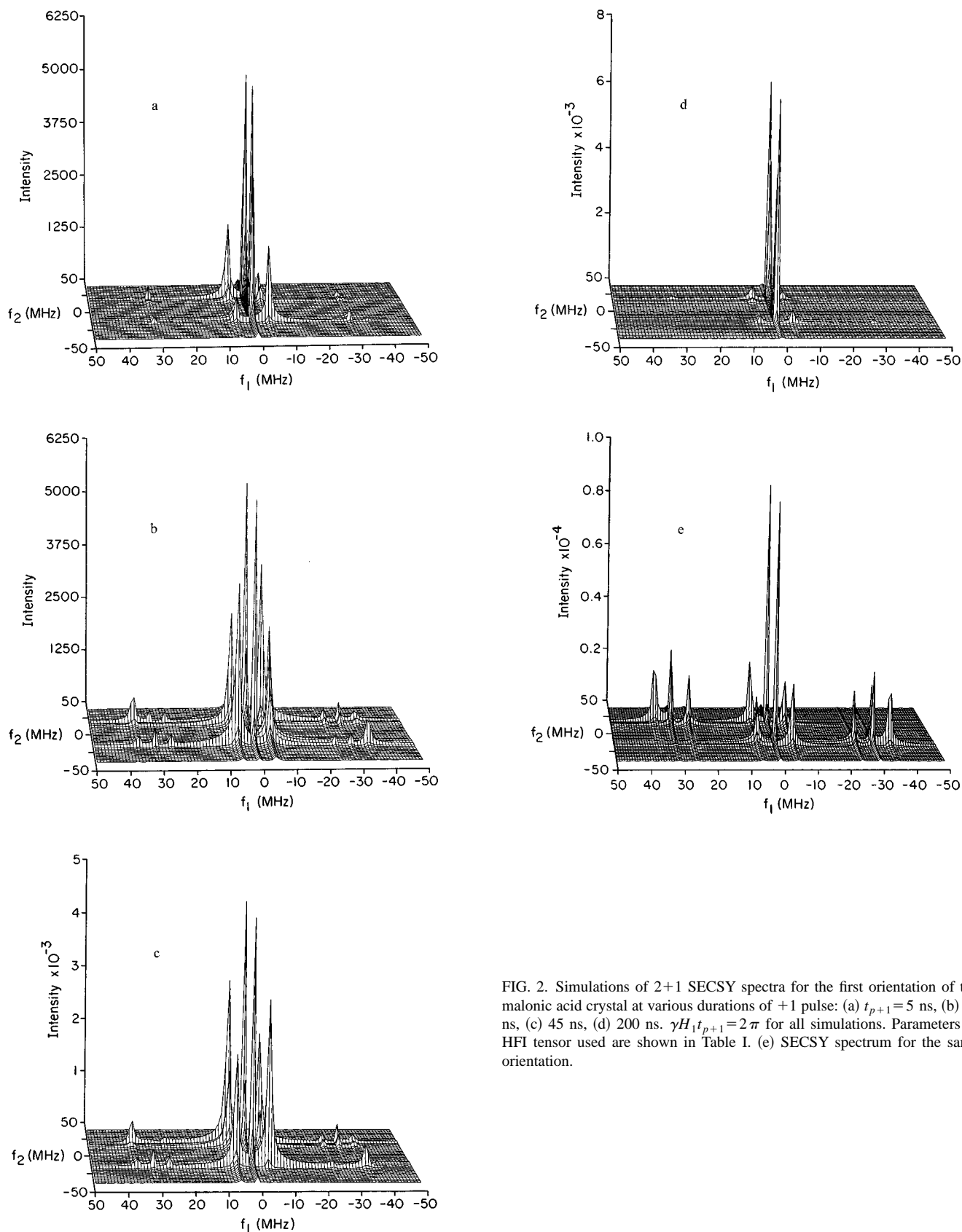


FIG. 2. Simulations of 2+1 SECSY spectra for the first orientation of the malonic acid crystal at various durations of +1 pulse: (a)  $t_{p+1} = 5$  ns, (b) 30 ns, (c) 45 ns, (d) 200 ns.  $\gamma H_1 t_{p+1} = 2\pi$  for all simulations. Parameters of HFI tensor used are shown in Table I. (e) SECSY spectrum for the same orientation.

These conditions are more conveniently applied for  $\Delta\omega \neq 0$ , so in all calculations the smallest value of  $\Delta\omega$  was kept equal to  $10^{-6}|\omega_\alpha - \omega_\beta|$  given that the calculated values of  $\omega_\alpha$  and  $\omega_\beta$  are accurate to better than  $10^{-9}$ . This allows one to simu-

$\omega_\beta$  are accurate to better than  $10^{-9}$ . This allows one to simulate a case of  $\Delta\omega = 0$  to high accuracy and to avoid a degeneracy of energies.

The procedure described above was first applied to a

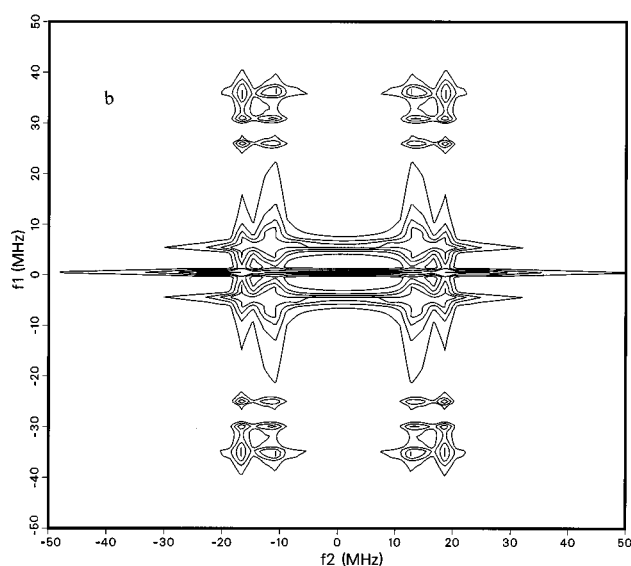
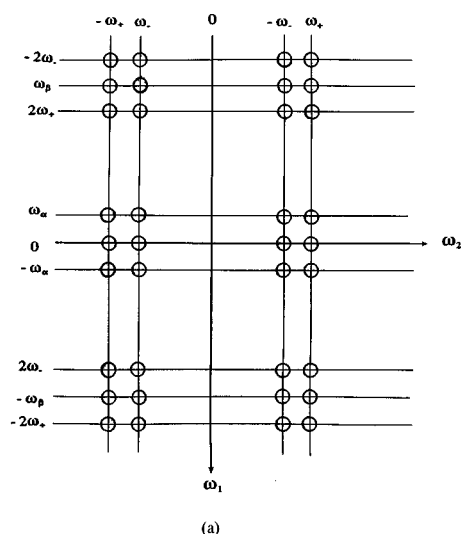


FIG. 3. (a) Schematic diagram for the 2+1 SECSY experiment. (b) Simulation of 2+1 SECSY: contour plot, first orientation,  $t_{p1}=30$  ns,  $\gamma H_1 t_{p1} = 2\pi$ .

number of cases with known analytical solutions in order to check the numerical calculations. In particular, we have calculated: the shapes of signals for two pulses and 2+1 pulse sequences with arbitrary pulse parameters (without HFI); SECSY simulations for the case of full excitation of the ESR spectrum; and the dependence of the nuclear modulation amplitude on pulse parameters for a two pulse train in the case of weak HFI ( $|B| \ll \omega_I$ ). The analytical solutions of these problems can be found in Refs. 8, 24, and 25. The numerical calculations were in good agreement with the calculations based on the corresponding analytical expressions for all cases.

The 2+1 SECSY simulations were performed in the following way. A typical fixed value for  $\tau$  of 1510 ns was chosen. This provides room for the second pulse position ( $t_1$ ) to be shifted through 256 steps of 5 ns each ranging from 130 to 1410 ns. The data collection of the echo shape typically ranged from  $\tau \pm 256$  ns in 256 steps of 2 ns. The number of the steps through  $t_2$  and  $t_1$  was chosen to be the same and

TABLE I. Parameters of HFI tensor used in calculations and fundamental frequencies of EPR transitions for the  $\alpha$  proton of the  $\text{CH}(\text{COOH})_2$  radical.<sup>a</sup>

| Crystal orientation<br>$\theta, \phi$ (deg) | $A$ (MHz) | $B^2$ (MHz <sup>2</sup> ) | $\omega_\alpha$ (MHz) | $\omega_\beta$ (MHz) |
|---|-----------|---------------------------|-----------------------|----------------------|
| 18, 0                                       | 32.6      | 100.0                     | 5.5                   | 30.7                 |
| 40, 0                                       | 41.8      | 203.0                     | 9.9                   | 35.6                 |

<sup>a</sup>The polar and azimuthal angles  $\theta$  and  $\phi$  are consistent with Ref. 8.

equal to 256. The first and third pulses, to simulate the experimental conditions, were  $90^\circ$  pulses with duration of 7.5 ns. The parameters of the +1 pulse were varied over a wide range of amplitudes and widths. The parameters of the HFI tensor corresponding to the experiments on irradiated malonic acid are shown in Table I. The details of determining  $A$  and  $B$  will be given in the experimental section. Except when otherwise needed, most calculations were performed for the case of  $\Delta\omega=0$ , which corresponded reasonably well to most of the experiments. To compare the calculated and experimental 2+1 SECSY spectra, a 2D-Fourier transformation of the measured and calculated time arrays was used. Some calculated 2D-2+1 SECSY spectra for the first set of HFI tensor parameters in Table I are shown in Figs. 2(a)–2(d). They correspond to  $2\pi$  rotations for the second pulse, which were achieved with different combinations of pulse width,  $t_{p2}$  and mw field strength  $\omega_{N2}$ . The 2D-SECSY spectrum calculated with the same HFI parameters is shown in Fig. 2(e) for comparison. Figure 3 is a contour map of the 2+1 SECSY spectrum of Fig. 2(b), which reveals the same set of frequencies as a SECSY experiment, i.e.,  $\omega_\alpha$ ,  $\omega_\beta$ ,  $\omega_\alpha + \omega_\beta$  and  $\omega_\alpha - \omega_\beta$ , in a slightly different manner (cf. Fig. 4 of Ref. 8). In particular, we get a doubling of the nuclear modulation peaks about the  $f_2=0$  axis. One clearly sees in Fig. 2, that the amplitude of the modulation cross peaks and the amplitude of the autopeaks depend on the parameters of the second pulse,  $\omega_{N2}$  and  $t_{p2}$ . In Fig. 2 we had fixed  $\omega_{N2} t_{p2} = 2\pi$ . Nevertheless, the modulation cross peaks depend on the duration of the +1 pulse. The cross peaks are a maximum for a +1 pulse duration equal to 30–45 ns and they decrease at higher  $t_{p2} = 200$  ns as well as at a smaller  $t_{p2} = 5$  ns. When the duration of the +1 pulse is optimal, the absolute intensity of the cross peaks at  $\omega_\alpha$  slightly exceeds the intensity of the same peaks in the SECSY spectrum at the same frequency [compare Figs. 2(b) and 2(c) with 2(e)].

Some 2+1 SECSY spectra for the second set of HFI tensor parameters are shown in Figs. 4(a)–4(d). In general, this set of simulations has the same features as the previous one: The intensity of the cross peaks depends on the duration of the +1 pulse, and at an optimal duration the relative intensity of the peaks at  $\omega_\alpha$  is 3–4 times higher than in the SECSY spectrum. The optimal pulse duration in this case is about 20 ns, because  $\omega_\alpha$  for this orientation is two times higher than in the first orientation (see Table I).

### III. EXPERIMENTAL METHODS

All experiments were performed on the Cornell 2D-FT-ESR spectrometer, which has been described in Refs. 8 and

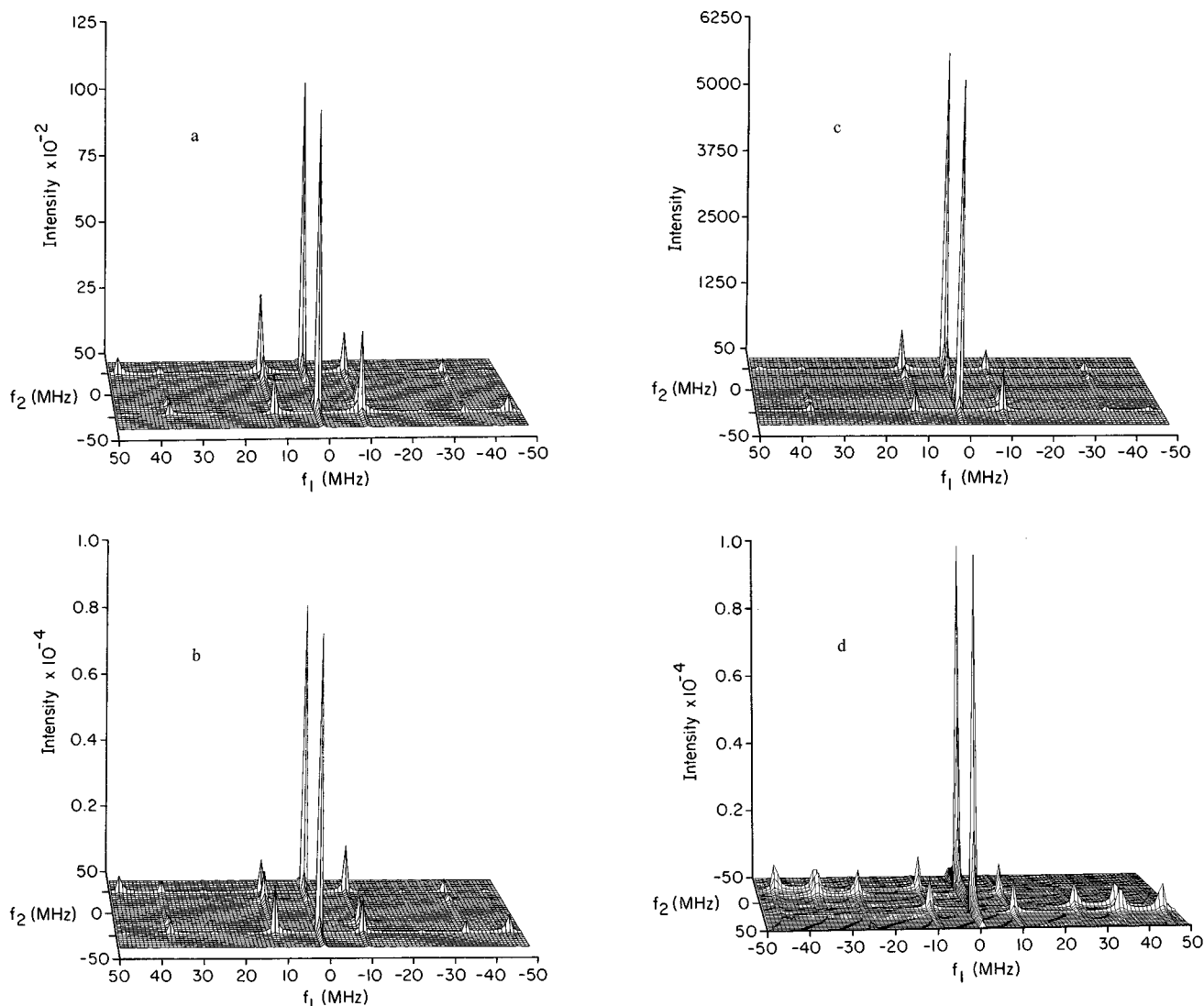


FIG. 4. Simulation of 2+1 SECSY spectra for the second orientation of the malonic acid crystal at various durations of the +1 pulse: (a)  $t_{p+1}=20$  ns, (b) 30 ns, (c) 45 ns.  $\gamma H_1 t_{p+1}=2\pi$  for all simulations. Parameters of HFI tensor used are shown in Table I. (d) SECSY spectrum of the same orientation.

28. For implementation of the 2+1 sequence, in which the +1 pulse amplitude must be independent of the first and the third pulses, the spectrometer was slightly modified.<sup>29</sup> The mw power from the klystron was divided into two channels. One of them was used for standard generation of the first and third pulses to drive the TWTA at full power. In the second channel we installed an additional switch and attenuator which allows one to change the duration and amplitude of the +1 pulse independent of the parameters of the first and third pulses. Then pulses from both channels were combined and directed to the TWTA. The duration of the first and third pulses of all 2+1 experiments reported here was constant and equal to 7.5 ns corresponding to a  $\pi/2$  pulse. (Normally 5 ns  $\pi/2$  pulses are to be expected with our spectrometer,<sup>8,11</sup> but the TWTA tube was aged and provided reduced gain.) The absolute values of the first and third pulse amplitudes were estimated by (i) observation of the primary spin-echo shape,<sup>30</sup> and by (ii) investigation of the dependence of the spin-echo amplitude in a two-pulse sequence on the pulse amplitude. These methods confirmed that 7.5 ns pulses pro-

vided a rotation angle of  $90^\circ \pm 5^\circ$ . The amplitude and duration of all three pulses were then sampled after the TWTA and were measured by an HP54100A digital oscilloscope. This permitted us to obtain the absolute amplitude of the +1 pulse by comparison with the amplitude of the first and third pulses. The minimal duration of the +1 pulse was chosen equal to 30 ns because it could deliver a  $2\pi$  pulse at maximum amplitude. Since our spectrometer<sup>28</sup> is specially designed for generation of very short pulses, the maximum pulse duration we could reach without major modification was about 200 ns.

The fixed distance between the first and third pulses in most experiments was equal to 1260 ns; the starting time interval between the first and +1 pulses was 150 ns; the step in  $t_1$  was chosen equal to 7 ns, the step in  $t_2$  was equal to 5 ns (or in some cases, 1 ns), and the entire collection over  $t_2$  consisted of 70 points or 350 ns. The acquisition time required for a single 2D experiment was about 1–2 h at about a 1 kHz repetition rate. (It is normally possible to operate at a 10 kHz repetition rate,<sup>8</sup> but we reduced this because of the

TABLE II. Phase cycle sequence for the 2+1 SECSY experiment.

| Step | Phases   |          |          | Memory address <sup>a,b</sup> |    |    |    |
|------|----------|----------|----------|-------------------------------|----|----|----|
|      | $\phi_1$ | $\phi_2$ | $\phi_3$ | 1                             | 2  | 3  | 4  |
| 1    | x        | x        | x        | 1                             | 2  |    |    |
| 2    | y        | y        | y        | 2                             | -1 |    |    |
| 3    | -x       | -x       | -x       | -1                            | -2 |    |    |
| 4    | -y       | -y       | -y       | -2                            | 1  |    |    |
| 5    | x        | y        | -x       | 1                             | 2  |    |    |
| 6    | y        | -x       | -y       | 2                             | -1 |    |    |
| 7    | -x       | -y       | x        | -1                            | -2 |    |    |
| 8    | -y       | x        | y        | -2                            | 1  |    |    |
| 9    | x        | -x       | x        | 1                             | 2  |    |    |
| 10   | y        | -y       | y        | 2                             | -1 |    |    |
| 11   | -x       | x        | -x       | -1                            | -2 |    |    |
| 12   | -y       | y        | -y       | -2                            | 1  |    |    |
| 13   | x        | -y       | -x       | 1                             | 2  |    |    |
| 14   | y        | x        | -y       | 2                             | -1 |    |    |
| 15   | -x       | y        | x        | -1                            | -2 |    |    |
| 16   | -y       | -x       | y        | -2                            | 1  |    |    |
| 17   | y        | x        | x        |                               |    | -1 | -2 |
| 18   | -x       | y        | y        |                               |    | -2 | 1  |
| 19   | -y       | -x       | -x       |                               |    | 1  | 2  |
| 20   | x        | -y       | -y       |                               |    | 2  | -1 |
| 21   | y        | y        | -x       |                               |    | -1 | -2 |
| 22   | -x       | -x       | -y       |                               |    | -2 | 1  |
| 23   | -y       | -y       | x        |                               |    | 1  | 2  |
| 24   | x        | x        | y        |                               |    | 2  | -1 |
| 25   | y        | -x       | x        |                               |    | -1 | -2 |
| 26   | -x       | -y       | y        |                               |    | -2 | 1  |
| 27   | -y       | x        | -x       |                               |    | 1  | 2  |
| 28   | x        | y        | -y       |                               |    | 2  | -1 |
| 29   | y        | -y       | -x       |                               |    | -1 | -2 |
| 30   | -x       | x        | -y       |                               |    | -2 | 1  |
| 31   | -y       | y        | x        |                               |    | 1  | 2  |
| 32   | x        | -x       | y        |                               |    | 2  | -1 |

<sup>a</sup>A table entry of  $-1$  signifies that the signal from the in phase arm of the dual quadrature detector is subtracted from that memory location. The contents of memory addresses 1 and 2, obtained from the two arms of the dual quadrature signal, form the real and imaginary parts, respectively, of  $S'$ , while addresses 3 and 4 give the real and imaginary parts of  $S''$ .

<sup>b</sup>In the results reported here we used the  $S_{c-}$  combination defined as  $S_{c-} = S' - iS''$  to sample the echo signal.

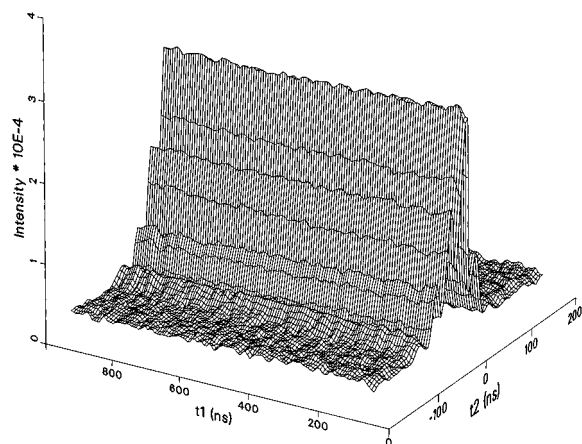


FIG. 5. Experimental time domain 2D array for 2+1 SECSY for the malonic acid crystal with a strongly attenuated +1 pulse showing the spectrometer stability.

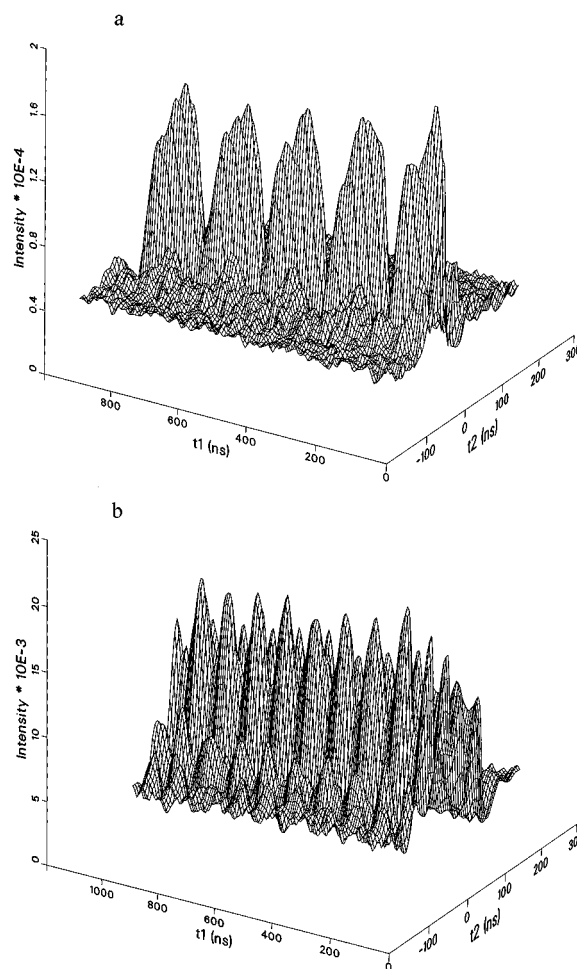


FIG. 6. Experimental time domain 2D array of 2+1 SECSY for the malonic acid crystal (a) first orientation,  $t_{p+1} = 45$  ns,  $\gamma H_1 t_{p+1} = 2\pi$ , (b) second orientation,  $t_{p+1} = 30$  ns,  $\gamma H_1 t_{p+1} = 1.32\pi$ .

aged TWTA tube.) To obtain just the primary spin-echo from the first and third pulses and to avoid any interference from unwanted echoes and free induction decays, a 32-step phase cycling sequence shown in Table II, was applied.

## IV. RESULTS

### A. $\text{CH}(\text{COOH})_2$ radicals in a malonic acid monocrystal

We first discuss results obtained on a single crystal of malonic acid with well defined faces and edges. The monocrystal was irradiated with Co-60 gamma rays with a dose of about 1 Mrad and aged for six months at room temperature. As is well known, such a soft annealing leaves just  $\text{CH}(\text{COOH})_2$  radicals; the less stable  $\text{CH}_2(\text{COOH})$  radicals disappear. The crystal was mounted on a specially designed delrin holder which was connected to a glass rod. The other end of the glass rod was attached to a goniometer. The crystal was oriented in such a way that the direction of the external field  $H_0$  and the  $z$  axis of the HFI tensor (in the definition of Ref. 8) were approximately perpendicular to each other and both were perpendicular to the goniometer axis. The measurements were performed for two orientations of the crystal with substantially different  $\omega_\alpha$  and  $\omega_\beta$  (see Table I). For each orientation, a SECSY experiment was performed

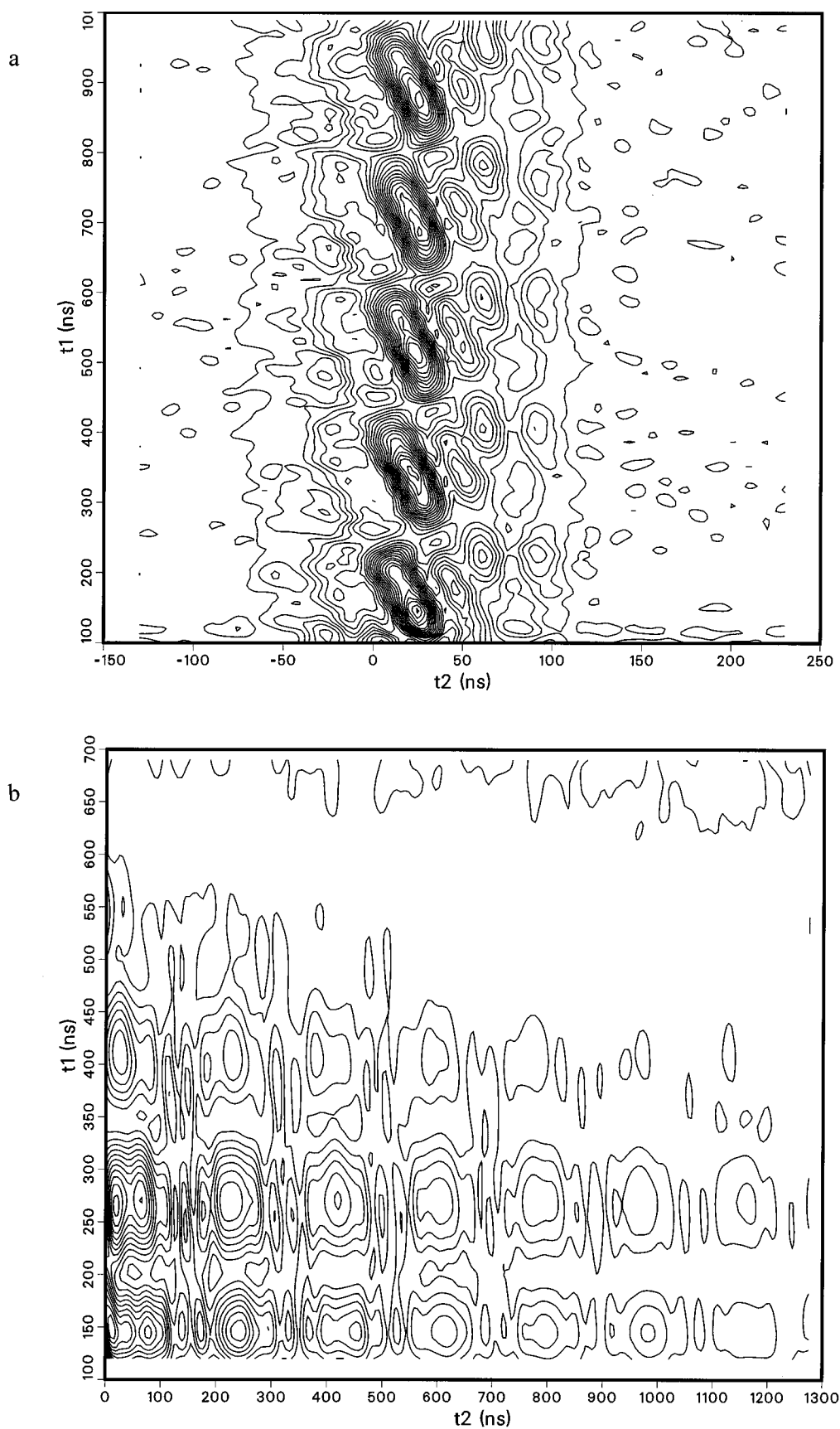


FIG. 7. (a) Contour plot of the time domain 2D array for 2+1 SECSY for the malonic acid crystal. First orientation,  $t_{p+1} = 45$  ns,  $\gamma H_1 t_{p+1} = 2\pi$ , (b) the time domain contour plot for SECSY at the same orientation.

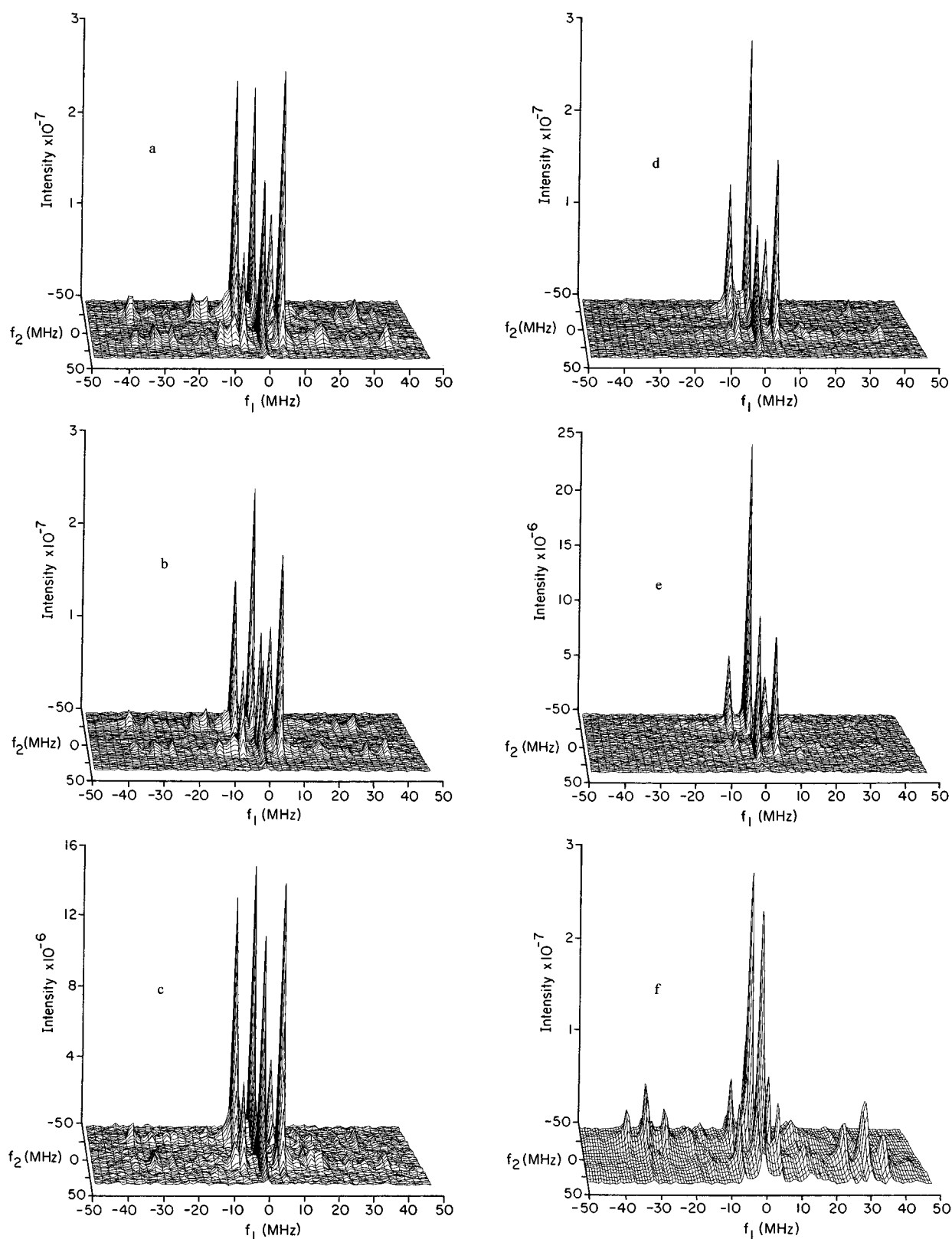


FIG. 8. Experimental 2+1 SECSY spectra for first orientation of the malonic acid crystal at various durations of +1 pulse: (a)  $t_{p+1} = 30$  ns, (c) 45 ns, (d) 60 ns, (e) 75 ns,  $\gamma H_1 t_{p+1} = 2\pi$ ; (b) 45 ns,  $\gamma H_1 t_{p+1} = 1.3\pi$ . (f) SECSY spectrum at the same orientation.

before the 2+1 SECSY experiment. A contour plot of the SECSY spectrum allowed us to obtain the values of  $\omega_\alpha$  and  $\omega_\beta$  to good accuracy. Then, having used the expressions of Eq. (2), we derived the Hamiltonian parameters, **A** and **B**

(Table I), which were used in our simulations of the 2+1 SECSY spectra. The mw frequency of the spectrometer and the external magnetic field  $H_0$  was chosen such that  $\Delta\omega \approx 0$  (more exactly  $\leq 3-4$  MHz). The precise value of  $\Delta\omega$  was

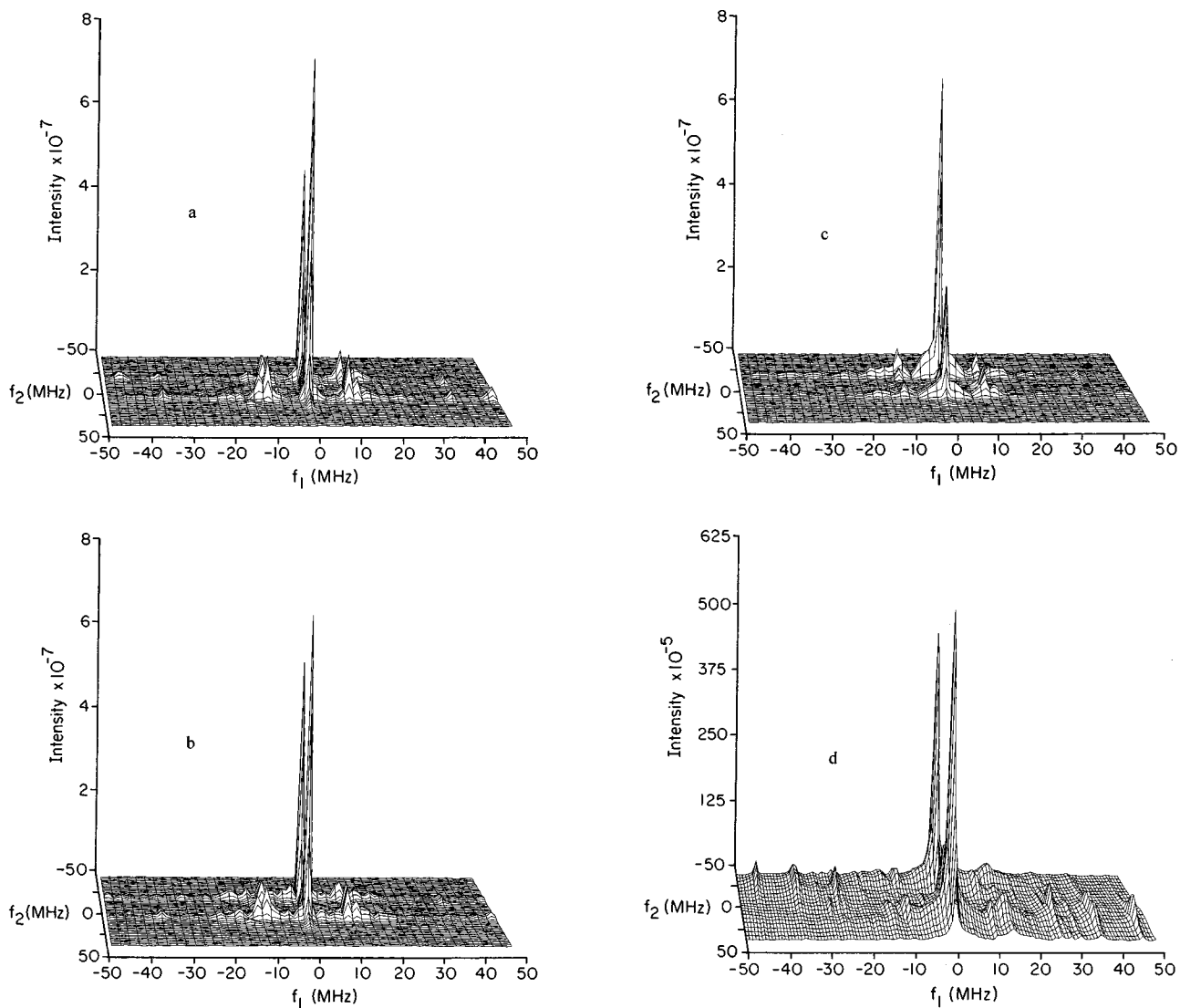


FIG. 9. Experimental 2+1 SECSY spectra for second orientation of the malonic acid crystal at various durations of +1 pulse: (a)  $t_{p+1}=30$  ns, (b) 45 ns, (c) 60 ns,  $\gamma H_1 t_{p+1}=2\pi$ . (d) SECSY spectrum of the same orientation.

determined by analyzing the contour map of the 2+1 SECSY spectra. The stability of the instrument in the course of data acquisition is demonstrated in Fig. 5. This is a representative 2+1 SECSY experiment, in which the +1 pulse was strongly attenuated. The weak modulation seen in Fig. 5 is caused by the residual +1 pulse. One notes that the amplitude instability during the course of the 1.5 h experiment was not more than 1%–2%.

Two representative 2+1 SECSY time domain results (magnitude data) are shown in Fig. 6. The data were collected with  $t_{p2}=45$  ns, and  $\omega_{N2}t_{p2}=2\pi$  for the first crystal orientation, and  $t_{p2}=30$  ns and the same rotation angle for the second orientation. The appearance of the time domain data in 2+1 SECSY differs from other techniques in an important way by the absence of any relaxation decay.<sup>16</sup> We compare the time domain behavior of 2+1 SECSY with the basic SECSY experiment in Fig. 7 in contour plots. [Note Fig. 7(a) corresponds to Fig. 6(a)]. The modulations appear as a series of ovals, whose principal axes are parallel to the  $t_1$  and  $t_2$  axes for SECSY [Fig. 7(b)], but they are tilted for

2+1 SECSY [Fig. 7(a)]. This leads to the result that different  $t_1$  slices have maxima at differing values of  $t_2$  for 2+1 SECSY (but not for SECSY), so that it is important to collect the full echo decay in  $t_2$  for each  $t_1$ , in order to accurately determine the modulation in the case of 2+1 SECSY. This feature arises from the nonfactorability of the nuclear modulation with respect to  $t_1$  and  $t_2$  discussed in connection with Eq. (19) for the case of a very weak modulation. Figure 7 shows that this is clearly also important for strong nuclear modulation.

Figures 8(a)–8(e) depicts a set of 2+1 SECSY spectra after 2D-FT of the time domain results which were collected at the first crystal orientation and for different parameters of the +1 pulse. The SECSY spectrum for the same orientation is shown in Fig. 8(f). As one can see from this figure the relative amplitude of the modulation cross peaks of 2+1 SECSY spectra at  $\omega_a$  substantially exceeds the relative amplitude of these peaks in the SECSY spectrum in agreement with the simulations of Fig. 2. (By relative amplitude we mean the amplitude of the cross peaks relative to that of the

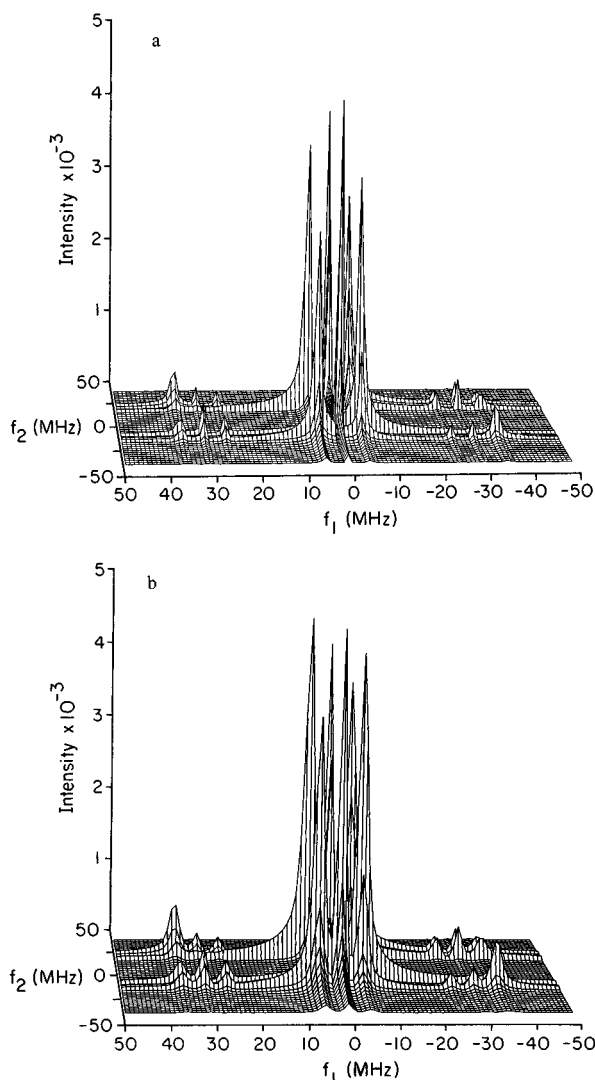


FIG. 10. Simulated 2+1 SECSY spectra for the malonic acid crystal, (a) first orientation,  $t_{p+1} = 30$  ns,  $\gamma H_1 t_{p+1} = 2\pi$ ,  $\Delta\omega = 3$  MHz; (b) the spectrum (a) convoluted with Gaussian  $\exp[-2\pi^2\Delta_G^2(t_1^2 + t_2^2)]$ . Linewidth  $\Delta_G = 1$  MHz in both dimensions.

autopeaks.) We discuss absolute amplitudes and sensitivity below. Also consistent with the simulations in Fig. 2, we observe that the amplitudes of the cross peaks decrease, at given  $t_{p2}$ , as the angle of rotation of the electron spins deviates from  $2\pi$ , [Fig. 8(b)]. They also decrease with increase of the pulse width when the angle of rotation is kept constant at  $2\pi$ . [Figs. 8(d) and 8(e)]. Similar behavior was observed for the second orientation of the crystal, and is shown in Figs. 9(a)–9(c), which is to be compared with the simulations of Fig. 4. We would like to point out that the 2+1 SECSY spectra at this orientation demonstrate the much better resolution of the  $\omega_\alpha$  frequency cross peaks, which are overlapped in the SECSY spectrum with the matrix proton cross peaks. The better resolution in the 2+1 SECSY experiment is a result of having much narrower spectral lines because of the absence of relaxation decay<sup>31</sup> and because of suppression of the matrix proton modulation at this particular pulse width. The narrowing of all peaks along  $f_1$  relative to SECSY is not evident in the simulations because they were all (including

SECSY) performed without any  $T_2$  (or  $T_1$ ) relaxation. Actually, the finite widths in the simulations and in the  $f_1$  direction for the experimental 2+1 SECSY autopeaks just arise from the FFT of a finite time signal in  $t_1$ . When extended to very long times,  $t_1$  the resolution in the  $f_1$  direction should become sharper, approaching infinitely sharp autopeaks and cross peaks whose widths reflect just the site variation in  $\omega_\alpha$  and  $\omega_\beta$ . Note that we could not reach the maximum amplitude of these cross peaks for the second orientation (due to our limits on available mw power); nevertheless the amplitude of the cross peaks exceeds that obtained in the SECSY experiment [compare Figs. 9(a) and 9(d)].

A comparison of the simulated and experimental spectra allows us to conclude that the simulations do correspond closely to the experiment but they depart from the experiment in some details. The probable reasons for the differences are the error in determining the rotation angle of the electron spins, the deviation of the pulse shape from rectangular, nonzero values of  $\Delta\omega$ , and inhomogeneous broadening of the EPR spectrum of the radical. In principle these features could be varied in the simulations till optimum fits are achieved, but the present computer program is quite time consuming. Therefore, in this paper we limited ourselves to less ambitious demonstrations of the effects of  $\Delta\omega$  and of the inhomogeneous broadening on the 2+1 SECSY spectra for a

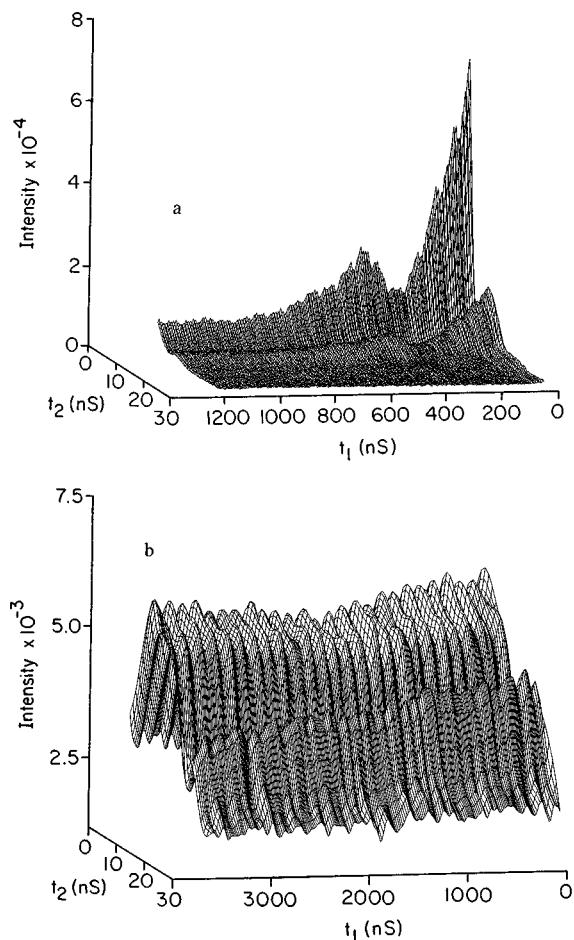


FIG. 11. (a) SECSY and (b) 2+1 SECSY time domain 2D arrays of frozen DPPH toluene solutions;  $t_{p+1} = 30$  ns,  $\gamma H_1 t_{p+1} = 2\pi$ . These are viewed almost end on along the  $t_2$  axis.

few cases. Figure 10(a) depicts the 2+1 SECSY spectrum calculated for the first orientation with  $\Delta\omega=3$  MHz,  $t_{p2}=30$  ns and  $\omega_{N2}t_{p2}=2\pi$ . As one can see from this figure, inclusion of the measured experimental value of  $\Delta\omega$  immediately gives the needed increase of cross-peak amplitude relative to the autopeaks, and therefore improves the agreement between simulations and experiments [compare Fig. 8(a) and Fig. 10(a)].

There are several sources of inhomogeneous broadening. If it is due to the interaction of the radical with surrounding protons, only a distribution in  $\Delta\omega$  needs to be included. Broadening caused by an orientational distribution of the radicals would lead to a distribution for  $A$  and  $B$  as well as for  $\Delta\omega$ , which can only be determined from superimposing simulations from several orientations to compare with experiment. For simplicity we included the first type of inhomogeneous broadening by multiplying Eq. (4) by the Gaussian  $\exp(-2\pi^2\Delta_G^2(t_1^2+t_2^2))$ . The resulting spectrum simulated with  $\Delta_G=1$  MHz [Fig. 10(b)] shows improved agreement with the experimental one. However, the introduction of a Gaussian inhomogeneous broadening along the  $f_1$  direction is unjustified because  $\Delta\omega$  broadening is cancelled in this direction by the spin-echo, but no improvement in the simulated spectrum is obtained if the Gaussian broadening with respect to  $t_1$  is removed. We believe that the better agreement of the relative intensities of auto and cross peaks for Fig. 10(b) hints at an artifact arising from the FFT. As noted above, an FFT of the finite time train can lead to a broadening along  $f_1$ . Specific features of the FFT appear to cause greater broadening of the modulation cross-peaks which occur at  $f_1 \neq 0$  than for the autopeaks occurring at  $f_1 = 0$ . Thus the addition of the artificial extra broadening tends to mask this difference, so the cross-peak amplitudes are enhanced relative to the autopeak amplitudes, as required to improve agreement with experiment. (We assume that white noise is the principal broadening feature along  $f_1$  in the experiments.) If this argument is justified, then it would imply that the dominant inhomogeneity in the experiment is a  $\Delta\omega$ -type inhomogeneity that probably relates to the matrix protons.

We now wish to make some comments about absolute signal strength and sensitivity of 2+1 SECSY vs SECSY. We have already shown that the relative amplitude of the cross peaks can be enhanced by 2+1 SECSY. A comparison of the experimental results of Fig. 8(c) (2+1 SECSY) with Fig. 8(f) (SECSY) shows that the autopeaks are reduced by a factor of ca. 2 in the 2+1 SECSY, whereas the intense cross peaks have been *enhanced* by a factor of ca. 2. The noise levels are comparable (although the 2+1 SECSY spectra were obtained in a mode, such that there are a greater density of points). A general analysis of the respective sensitivities depends on many parameters including the value of  $T_2$ , the line shapes, and the HFI. For the case of Fig. 8, we had a  $1.5 \mu\text{s}$  separation between the first and third pulses. With a  $T_2 \sim 0.8 \mu\text{s}$ , this meant that the 2+1 SECSY signal was obtained at a constant value of 0.15 in arbitrary units. For SECSY, we used the same time interval for data acquisition, so the signal amplitude varied from 1 to 0.15, which yields an average amplitude of 0.45. Thus it is not surprising that the amplitude of the autopeaks were reduced in the 2+1 SECSY experi-

ment. On the other hand, the sharpening up of the auto- and cross peaks along the  $f_1$  axis for 2+1 SECSY, due to cancellation of  $T_2$  broadening, is a mechanism that enhances the signal-to-noise of the 2+1 SECSY signal. Linear predictive methods of data processing<sup>11,12</sup> instead of FFT could help to remove the artificial broadening along  $f_1$  due to the “FFT-ing” of a finite time train.

## B. DPPH in frozen toluene solution

In the previous example we illustrated the ability of 2+1 SECSY to provide relative enhancement of modulation effects. In the next example we consider the opposite case, i.e., a suppression of modulation. The SECSY time domain signal from a frozen solution of DPPH in toluene is shown in Fig. 11(a) which is an end-on view along  $t_1$ . The experiment was performed at  $-110$  °C and the DPPH concentration was  $10^{18}$   $\text{cm}^{-3}$ . The modulation of the spin-echo signal which is observed in Fig. 11(a) has previously been reported,<sup>32</sup> and it is due to the HFI of the electron spin with the nitrogen nuclei of the radical (the deep and low-frequency modulation) and with neighboring protons of the matrix (the shallow and high-frequency modulation). A 2+1 SECSY signal, collected for the same sample, is shown in Fig. 11(b). The +1 pulse duration in this experiment was equal to 30 ns, corresponding to a rotation angle of  $2\pi$ . One can see from the 2D format in Fig. 11(b) that in this 2+1 SECSY experiment the modulation from the nitrogen nuclei is not observed, and the signal is modulated just by the proton frequency of 14 MHz. Thus Figs. 11 shows that 2+1 SECSY allows one to select the modulation frequency in a way that is opposite to more traditional spin-echo techniques. The traditional techniques using “soft pulses” (partial excitation) allow one to suppress the high-frequency component of modulation. To our knowledge, none of the existing techniques can leave the high-frequency part of the modulation, while suppressing the low-frequency part. Given that the modulation of the signal is generated during the action of the +1 pulse in 2+1 SECSY, then if the duration of this pulse is not long enough for a given frequency, no modulation is observed. For this particular case of a  $^{14}\text{N}$  modulation frequency  $\sim 1$  MHz, the +1 pulse duration has to be about  $1 \mu\text{s}$ . In the present experimental setup, the maximum +1 pulse duration which we could achieve was 150 ns, and that was not sufficient to demonstrate the opposite situation predicted by theory, viz. suppression of the 14 MHz proton modulation and enhancement of the 1 MHz  $^{14}\text{N}$  modulation. With a +1 pulse duration of 150 ns, we observed the virtual disappearance of both modulation patterns. The effect of suppression of modulation by a 2+1 pulse sequence was used in Refs. 13 and 33 in different samples for the investigation of dipole–dipole interactions between electron spins.

The present example enables us to illustrate how the method might be applied to the determination of the local nuclear environment of paramagnetic centers (e.g., paramagnetic centers in biological molecules, catalysts, metallo-organic compounds and in radiation-induced paramagnetic centers). The characteristic parameters that are used for determining the structure of the local nuclear environment of paramagnetic centers are (i) the amplitude of modulation, (ii)

the modulation frequencies, and (iii) the time constant for the modulation decay. In simple systems wherein just a single kind of nucleus is in the vicinity of the paramagnetic center, traditional methods are sufficient.<sup>34–36</sup> However, even for a relatively simple system such as DPPH, these methods do not work very well. It is not practical to obtain the decay time of the proton modulation from the data shown in Fig. 11(a). However, with the 2+1 experiment, in which relaxation decay and the modulation from the nitrogen nuclei are absent, this is easily obtained. Furthermore, the dependence of the modulation on the +1 pulse parameters may be used for verification of the assignments, as previously shown for a simple case in Ref. 16.

For our case of DPPH in frozen toluene solution, a simple evaluation of the average proton distance may be obtained directly from the experiment. First of all the absence of modulation decay in time interval  $t_1$  allows us to believe that the component  $T_{zz}$  of the anisotropic proton HFI tensor,<sup>1,2</sup> which is responsible for this decay,<sup>35</sup> is less than 1 MHz. ( $T_{zz}$ ,  $T_{zx}$ ,  $T_{zy}$  is a common notation for the components of the tensor of dipolar electron–nuclear interaction, see, e.g., Refs. 1 and 2.) Since the other components of the anisotropic part of the HFI tensor are less than  $T_{zz}$ , the modulation is caused by a weak interaction, where  $T_{zz}$ ,  $T_{zx}$ ,  $T_{zy} \ll \omega_n$ . It allows us to conclude that the low-frequency modulation observed in Fig. 11(b) is caused by a slight deviation of  $\omega_\alpha$  and  $\omega_\beta$  from  $\omega_n$ ; where, for weak interaction, one has from Eq. (2)  $\omega_\alpha$ ,  $\omega_\beta = \omega_n \pm T_{zz}/2$ . Taking into account the time-dependent portion of Eq. (19), we performed a simple simulation of the modulation pattern in Fig. 11(b) and evaluated  $T_{zz}$  as 0.4–0.35 MHz which corresponds to the average proton–electron distance of about 4.5–5 Å. Of course, this is a very approximate estimate, but it does illustrate how easily the data may be used to obtain structural information from the modulation pattern.

## V. SUMMARY

The 2+1 SECSY experiment is an example of what we call pulse adjustable spectroscopy, because it introduces the pulse width and pulse amplitude as adjustable parameters, which enable one to tune in and/or tune out key features of the spin echoes and the nuclear modulation in order to enhance resolution to features of interest. In particular, it permitted preferential enhancement of the nuclear modulation cross peaks ( $\omega_\alpha$ ) relative to the autopeaks in the case of irradiated malonic acid with a large proton HFI. It also permitted the suppression of the matrix proton peaks. In this spirit, we have also shown how to significantly suppress the autopeaks, thereby improving the resolution to low-frequency cross peaks. In the case of DPPH in a glass, we could suppress the low-frequency  $^{14}\text{N}$  nuclear modulation, leaving just the matrix  $^1\text{H}$  nuclear modulation. We wish to emphasize that this is the only single-frequency technique whereby low-frequency modulations can be suppressed and high frequency modulation retained. These features are important in powders or disordered materials for cases where there are several nuclei providing the modulation, since this enables a more accurate assessment of the modulation decay associated with each type of nucleus. Equally important for

improving resolution to the modulation decay, is the greatly enhanced resolution, compared to SECSY, in the  $f_1$  frequency direction, because the decay in  $T_2$  has been removed. It is this modulation decay that is the principal source of distance measurements in ESEEM experiments,<sup>1,2</sup> and it now appears as the dominant feature in the broadening of the 2+1 SECSY widths vs  $f_1$  provided one has sampled a wide enough range of the time,  $t_1$ , between the first and the +1 pulse.

The particular virtues of performing the 2+1 pulse sequence in a 2D format as 2+1 SECSY include the following. First of all, it provides the ability (at least for single crystals) of correlating the modulation cross peaks in order to improve the ability to make assignments when there are several types of radical. This feature is very similar to that for 2D correlation spectroscopy in NMR.<sup>37</sup> A general feature of the 2+1 pulse sequence (and we suspect for other pulse adjustable sequences), is that the modulation does not simply factorize as a product of separate functions of  $t_1$  and  $t_2$  [cf. Fig. 7(a)]. Thus we do not know precisely where, in the spin-echo, the modulation is most prominent, and this feature changes with  $t_1$ . In the 2+1 SECSY format the full spin-echo shape is explicitly recorded, thereby avoiding any ambiguities in the analysis. It occurs to us that for powder spectra, a useful representation of the 2+1 SECSY nuclear modulation peaks can be obtained by projecting the 2D magnitude spectrum onto the  $f_1$  axis (i.e., integrating the spectrum over  $f_2$ ) to obtain the full spectral contribution to each modulation peak. However, specific, potentially useful features of the 2D peak shapes could be lost. 2+1 SECSY differs from SECSY in that it is insensitive to spin relaxation, a desirable feature in studying the nuclear modulation, as we have stressed. Even if spin relaxation is of interest, it would seem advisable to carefully characterize the nuclear modulations using 2+1 SECSY and then to return to SECSY to examine the additional features ascribable to spin relaxation.

Finally, we wish to point out the extremely good agreement between theory and experiment demonstrated for the case of the malonic acid single crystal. It would imply that this experiment has been well characterized, so that it could be effectively implemented to study other systems of single crystals or disordered solids.

## ACKNOWLEDGMENTS

This work was supported by NIH Grant No. RR07126 and NSF Grant No. CHE9313167. We wish to thank Dr. Baldev Patyal for his help with the malonic acid single crystals and Dr. Sanghyuk Lee for his help in determining the phase cycling utilized in this work. A preliminary account of this work was presented at the 17th International EPR Symposium in Denver, August, 1994.

<sup>1</sup> *Modern Pulsed and Continuous-Wave Electron Spin Resonance*, edited by L. Kevan and M. K. Bowman (Wiley, New York, 1990).

<sup>2</sup> S. A. Dikanov and Y. D. Tsvetkov, *Electron Spin Echo Envelope Modulation (ESEEM) Spectroscopy* (Chemical Rubber, Boca Raton, 1992).

<sup>3</sup> P. Höfer, A. Grupp, H. Nebeführer, and M. Mehring, *Chem. Phys. Lett.* **132**, 279 (1986).

<sup>4</sup> C. Gemperle, G. Aebi, A. Schweiger, and R. R. Ernst, *J. Magn. Reson.* **88**, 241 (1990).

- <sup>5</sup>C. Gemperle, A. Schweiger, and R. R. Ernst, *Chem. Phys. Lett.* **178**, 565 (1991).
- <sup>6</sup>A. Schweiger, C. Gemperle, and R. R. Ernst, *J. Magn. Reson.* **86**, 70 (1990).
- <sup>7</sup>L. Braunschweiler, A. Schweiger, J. M. Fauth, and R. R. Ernst, *J. Magn. Reson.* **64**, 160 (1985).
- <sup>8</sup>S. Lee, B. R. Patyal, and J. H. Freed, *J. Chem. Phys.* **98**, 3665 (1993).
- <sup>9</sup>J. H. Freed, *J. Chem. Soc. Faraday Trans.* **86**, 3173 (1990).
- <sup>10</sup>D. Gamliel and J. H. Freed, *J. Magn. Reson.* **89**, 60 (1990).
- <sup>11</sup>B. R. Patyal, R. H. Crepeau, D. Gamliel, and J. H. Freed, *Chem. Phys. Lett.* **175**, 445 (1990).
- <sup>12</sup>J. Gorcoster, G. L. Millhauser, and J. H. Freed, in *Advanced EPR*, edited by A. J. Hoff (Elsevier, Amsterdam, 1989).
- <sup>13</sup>V. V. Kurshev, A. M. Raitsimring, and Yu. D. Tsvetkov, *J. Magn. Reson.* **81**, 441 (1989).
- <sup>14</sup>M. K. Bowman, *Isr. J. Chem.* **32**, 31 (1992).
- <sup>15</sup>M. K. Bowman, R. J. Massoth, and C. S. Yannoni, in *Pulsed Magnetic Resonance: NMR, ESR and Optics*, edited by D. M. S. Bagguley (Clarendon, Oxford, 1992).
- <sup>16</sup>V. V. Kurshev, A. V. Astashkin, and A. M. Raitsimring, *Zh. Struct. Khim.* **29**, 73 (1988) [Engl. trans.: *J. Struct. Chem.* **29**, 62 (1988)].
- <sup>17</sup>V. F. Yudanov, A. M. Raitsimring, and Yu. D. Tsvetkov, *Teor. Eksp. Khim.* **4**, 520 (1968) [Engl. trans.: *Theor. Exp. Chem.* **4**, 338 (1968)].
- <sup>18</sup>H. Thomann and M. Bernardo, *Spectrosc. Int. J.* **8**, 119 (1990).
- <sup>19</sup>H. M. McConnell, C. Heller, T. Cole, and R. W. Fessenden, *J. Am. Chem. Soc.* **82**, 766 (1960).
- <sup>20</sup>W. B. Mims, *Phys. Rev. B* **5**, 2409 (1972).
- <sup>21</sup>W. B. Mims, *Phys. Rev. B* **6**, 3543 (1972).
- <sup>22</sup>We use  $\mathbf{S}^+$  for notational convenience. More accurately it should be the associated magnetization operator, but following Mims we reserved  $\mathbf{M}$  and  $\mathbf{M}^+$  for other operators defined below.
- <sup>23</sup>M. K. Bowman and R. J. Massoth, in *Electronic Magnetic Resonance of the Solid State*, edited by J. A. Weil (Canadian Society for Chemistry, Ottawa, 1987), p. 99.
- <sup>24</sup>A. Bloom, *Phys. Rev.* **98**, 1104 (1955).
- <sup>25</sup>A. V. Astashkin, S. A. Dikanov, V. V. Kurshev, and Yu. D. Tsvetkov, *Chem. Phys. Lett.* **136**, 335 (1987).
- <sup>26</sup>H. Barkhuijsen, R. de Beer, B. J. Pronk, and D. van Ormondt, *J. Magn. Reson.* **61**, 284 (1985).
- <sup>27</sup>W. M. Press, B. P. Flannery, S. A. Teukolsky, and W. T. Vetterling, *Numerical Recipes* (Cambridge University, New York, 1987).
- <sup>28</sup>J. Gorcoster and J. H. Freed, *J. Chem. Phys.* **88**, 4678 (1988).
- <sup>29</sup>J. Gorcoster, G. L. Millhauser, and J. H. Freed, in *Modern Pulse and Continuous Wave Electron Spin Resonance*, edited by L. Kevan and M. K. Bowman (Wiley, New York, 1990).
- <sup>30</sup>A. M. Raitsimring and K. M. Salikhov, *Bull. Magn. Reson.* **7**, 184 (1985).
- <sup>31</sup>Note that in 2+1 SECSY the relaxation decay is rigorously independent of the time,  $t_1$ . That is, to correct Eq. (10) for relaxation we would have to multiply it by the factor  $\exp[-T_{2,e}^{-1}(2\tau+t_2)+\tilde{T}_{2,e}^{-1}t_{p2}]$  where we recognize that this echo signal results from the spins that remain in the rotating  $x-y$  plane after the first pulse and are therefore subject to  $T_{2,e}$  relaxation. We also allow for the possibility that there is a modified  $T_{2,e}$  (given by  $\tilde{T}_{2,e}$ ) during the second pulse of duration  $t_{p2}$ . The important point is that this factor is independent of  $t_1$ .
- <sup>32</sup>H. L. Flanagan, G. J. Gerfen, and D. J. Singel, *J. Chem. Phys.* **88**, 20 (1988).
- <sup>33</sup>V. V. Kurshev, A. M. Raitsimring, and K. M. Salikhov, *Sov. Phys. Solid State* **30**, 139 (1988).
- <sup>34</sup>D. A. Narayana, D. Suryanarayana, and L. Kevan, *J. Am. Chem. Soc.* **104**, 3552 (1982).
- <sup>35</sup>A. V. Astashkin, S. A. Dikanov, and Yu. D. Tsvetkov, *Chem. Phys. Lett.* **144**, 258 (1988).
- <sup>36</sup>Z. Levi, A. M. Raitsimring, and D. Goldfarb, *J. Phys. Chem.* **95**, 7830 (1990).
- <sup>37</sup>R. R. Ernst, G. Bodenhausen, and A. Wokaun, *Principles of Nuclear Magnetic Resonance in One and Two Dimensions* (Oxford, New York, 1987).